Title: Reactive Oxygen Species Regulate Activity-Dependent Neuronal Structural Plasticity in *Drosophila*

Authors: Matthew C. W. Oswald[1*], Paul S. Brooks[1], Maarten F. Zwart[2], Amrita Mukherjee[1], Ryan J. H. West[3], Khomgrit Morarach[1], Sean T. Sweeney[3], Matthias Landgraf[1*]

*Correspondence to: mo364@cam.ac.uk and ml10006@cam.ac.uk

Affiliations:

[1] University of Cambridge, Department of Zoology, Downing Street, Cambridge, CB2 3EJ, United Kingdom

[2] HHMI Janelia Research Campus, Ashburn, VA, 20147, USA

[3] Department of Biology, University of York, Heslington York YO10 5DD, United Kingdom

Abstract

Neurons are inherently plastic, adjusting their structure, connectivity and excitability in response to changes in activity. How neurons sense changes in their activity level and then transduce these to structural changes remains to be fully elucidated. Working with the *Drosophila* larval locomotor network, we show that neurons use reactive oxygen species (ROS), metabolic byproducts, to monitor their activity. ROS signals are both necessary and sufficient for activity-dependent structural adjustments of both pre- and postsynaptic terminals and for network output, as measured by larval crawling behavior. We find the highly conserved Parkinson's disease-linked protein DJ-1ß acts as a redox sensor in neurons where it regulates pre- and postsynaptic structural plasticity, in part via modulation of the PTEN-PI3Kinase pathway. Neuronal ROS thus play an important physiological role as second messengers required for neuronal and network tuning, whose dysregulation in the ageing brain and under neurodegenerative conditions may contribute to synaptic dysfunction.

Introduction

Plasticity is fundamental to neuronal development and function. Changes in activity can trigger a raft of different responses, including changes to synaptic size, strength and connectivity, as well as to neuronal excitability (Davis and Müller, 2015; Keck et al., 2017; Wefelmeyer et al., 2015). 'Hebbian' plasticity mechanisms, such as long-term potentiation or depression, lead to altered transmission strength. These are balanced by homeostatic mechanisms, which are compensatory in nature and work toward maintaining neuronal or network activity within a set range. For example, blockade of excitatory inputs in neurons can induce a range of changes that are compensatory, including enlargement of both pre- and post-synaptic specializations, increasing synapse, axonal bouton and dendritic spine number as well as reducing dendritic spine elimination (Burrone et al., 2002; Kirov and Harris, 1999; Murthy et al., 2001; Zuo et al., 2005). How neurons monitor their activity levels is not known. Models of action potential firing rate homeostasis suggest that neurons measure the frequency of action potential firing and use homeostatic plasticity mechanisms to maintain this within their set point range (Davis, 2006; Turrigiano, 2012). In support of this view, recent studies in the mammalian visual system demonstrated that following dramatic activity disturbances, such as monocular occlusion, different types of neurons do indeed return to their original cell type-specific firing rate (Hengen et al., 2013; 2016).

An important second messenger in the regulation of activity-dependent plasticity is calcium, whose intracellular concentration correlates with neuronal activity patterns. Calcium regulates cellular and synaptic changes through a raft of signaling pathways, cytoskeletal and transcriptional effector proteins, including calcium/calmodulin-dependent protein kinase II (CaMKII), the phosphatase calcineurin and cyclic nucleotide signaling pathways (Vonhoff and Keshishian, 2017).

Here, we considered whether neurons might also monitor their activity levels by utilizing other signals. Neuronal activity levels correlate with energetic demand, suggesting that signals associated with energy metabolism could in principle provide a proxy measure for activity (Attwell and Laughlin, 2001; Hallermann et al., 2012; Zhu et al., 2012). We

62 therefore focused on reactive oxygen species (ROS), which are formed as obligate byproducts
63 of mitochondrial respiratory ATP synthesis; ROS form by 'leakage' of the electron transport
64 chain, which leads to the generation of superoxide anions (O_2^-), and hydrogen peroxide
65 (H_2O_2) (Halliwell, 1992). Intensively studied as destructive agents when at high
66 concentration in the context of ageing and neurodegenerative conditions, in healthy cells
67 ROS are necessary for many physiological processes, including growth factor signaling
68 (Finkel, 2011). In cultured neurons, mitochondrial O_2^- production can be triggered by field
69 stimulation (Hongpaisan et al., 2004; 2003). Increase in neuronal ROS levels were also
70 reported following NMDA receptor stimulation, reportedly generated by mitochondria
71 (Bindokas et al., 1996; Dugan et al., 1995) and NADPH oxidases (Brennan et al., 2009). In
72 hippocampal and spinal cord slices, ROS were found sufficient and necessary for inducing
73 'Hebbian' forms of plasticity (LTP) (Kamsler and Segal, 2003a; 2003b; Klann, 1998; Knapp
74 and Klann, 2002; Lee et al., 2010); and mice that over-express superoxide dismutase showed
75 defects in hippocampal LTP and learning paradigms (Gahtan et al., 1998; Levin et al., 1998;
76 Thiels et al., 2000).

77 To explore whether neurons might use metabolic ROS as signals for activity-induced
78 structural plasticity, we used as a model the motor system of the fruitfly larva, *Drosophila*
79 *melanogaster*, which is composed of individually identifiable motoneurons located in the
80 ventral nerve cord and their specific target muscles in the periphery (Kohsaka et al., 2012).
81 We had previously shown that ROS can regulate neuromuscular junction (NMJ) structure
82 (Milton et al., 2011). Here, we show that the locomotor network of the *Drosophila* larva
83 undergoes homeostatic adjustment in response to prolonged overactivation, as measured by
84 larval crawling, its physiological output. This homeostatic adjustment of the network
85 includes and requires structural plasticity of synaptic terminals. We show that ROS
86 signaling, H_2O_2 in particular, is necessary and sufficient for this activity-induced synaptic
87 terminal plasticity, of both presynaptic NMJ terminals and postsynaptic dendritic arbors
88 within the central nervous system (CNS). As a sensor for activity-generated ROS we
89 identified the conserved redox sensitive protein DJ-1ß, a homologue of vertebrate DJ-1

90 (PARK7) (Meulener et al., 2005). DJ-1ß genetically interacts with the phosphatase and
91 tensin homolog (PTEN) and upon ROS mediated oxidation disinhibits PI3kinase signaling at
92 the presynaptic NMJ, thus promoting synaptic terminal growth, as seen with activity-
93 induced potentiation. Strong over-activation on the other hand leads to DJ-1ß-dependent
94 compensatory adjustments of reduced release sites presynaptically and smaller dendritic
95 input arbors.
96
97
98

99 # Results

100 ## Induction of prolonged activity leads to homeostatic adjustment in the larval
101 ## *Drosophila* motor network

102 Neural circuits are inherently plastic and capable of adjusting their output with behavioral
103 need. Our aim was to investigate mechanisms that allow neurons to sense changes in their
104 activity levels and in response mediate adaptive structural adjustments. As an experimental
105 model we used the locomotor network of the *Drosophila* larva, whose motoneurons grow
106 dramatically over the course of larval life and are known to be plastic (Budnik et al., 1990;
107 Davis, 2006; Schuster et al., 1996; Tripodi et al., 2008; Zito et al., 1999; Zwart et al., 2013). A
108 simple way of manipulating activity in the locomotor network of *Drosophila* larvae is by
109 changing ambient temperature (Dillon et al., 2009; Sigrist et al., 2003; Zhong and Wu,
110 2004). As previously documented (Sigrist et al., 2003; Zhong and Wu, 2004), we found that
111 network activity increased upon *acutely* shifting animals to higher ambient temperatures
112 (e.g. from 25°C to 29°C or 32°C), resulting in increased larval crawling speeds (Figure 1A). In
113 contrast, following *prolonged* exposure to higher temperatures (rearing at 29°C and 32°C)
114 we found that larvae crawled at the same speed as controls kept at 25°C (grey horizontal
115 dotted line in Figure 1A), suggestive of homeostatic network adjustment. Mechanistically,
116 neurons might compensate for the increased network drive that is the result of higher
117 temperatures by reducing their individual excitability and/or synaptic input, thus returning
118 motor output to the default crawling speed. In agreement with this model, when 29°C and
119 32°C-conditioned larvae were *acutely* shifted to a lower temperature of 25°C they displayed
120 reduced crawling speed (green data in Figure 1a), with 32°C-adjusted larvae crawling
121 significantly slower than 29°C -adjusted animals.

122 To test this further, we selectively over-activated the glutamatergic motoneurons by
123 mis-expression of the warmth-gated cation channel dTrpA1 and rearing these animals at
124 27°C, a temperature that robustly activates dTrpA1-expressing neurons (Hamada et al.,
125 2008; Pulver et al., 2009). Upon *acute* removal of this motoneuron over-stimulation (by

126 shifting to 22°C, where the dTrpA1 channel is closed) larval crawling speed reduced
127 significantly relative to non-dTrpA1 expressing controls (Figure 1B). Thus, prolonged
128 increase of network drive leads to homeostatic adjustment that returns network output, and
129 thus larval crawling speed, to a default set point. Cell type-selective manipulations of the
130 motoneurons, which constitute the output of the motor network, show that they are major
131 contributors to this adjustment.

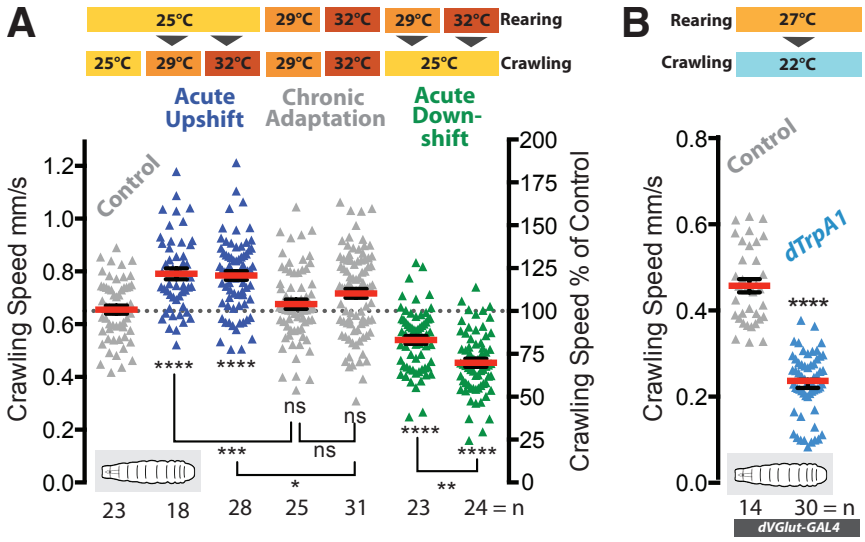

Figure 1: Adaptive behavioral plasticity is response to chromic locomotor over-activation. (**A**) Larval motor network activity, assayed by crawling speed 72hrs after larval hatching (ALH), increases in response to acute temperature upshifts (blue) in wild type larvae (Oregon R = control in all conditions). In contrast, with prolonged exposure (grey) to elevated temperatures (29°C or 32°C) the motor network adapts homeostatically generating the same crawling speed as 25°C reared controls. This adaptation is further revealed by acute temperature downshifts (green). Each data point represents crawling speed from an individual uninterrupted continuous forward crawl, n = specimen replicate number, up to 3 crawls assayed for each larva. Mean +/- SEM, ANOVA, ns = not significant, *P<0.05, **P<0.01, ***P<0.001, ****P<0.0001 (**B**) Prolonged over-activation targeted to motoneurons (*dVGlut-GAL4*; *UAS-dTrpA1*) also leads to adaptation with reduced crawling speed (dTRPA1 channels open at 27°C, closed at 22°C). Mean +/- SEM, control is *dVGlut-GAL4 / +*. ****P<0.0001 students t test, n = replicate number.

132

133 **Structural plasticity of synaptic terminals is regulated by activity**

134 We then asked what structural changes within the network might be associated and
135 potentially responsible for these homeostatic behavioral adjustments. To this end, we
136 focused on two well characterized motoneurons, 'aCC' and 'RP2' (Choi et al., 2004; Landgraf
137 et al., 2003). Their presynaptic neuromuscular junction (NMJ) terminals consist of varicose
138 compartments (boutons) strung across the muscle surface, each containing multiple
139 synapses in the form of active zones (Van Vactor and Sigrist, 2017) (Figure 2A). We found
140 that increases in motor network activity stimulated by higher ambient temperatures (raising
141 animals at 29°C or 32°C) led to more, albeit smaller boutons at the NMJ by the wandering
142 third instar larval stage, 100 hrs after larval hatching (ALH) (Figure 2C, grey data) (Sigrist et
143 al., 2003; Zhong and Wu, 2004). To exclude non-specific effects, we targeted over-activation
144 selectively to the aCC and RP2 motoneurons, via expression of the warmth-gated ion channel
145 dTrpA1, and found similar presynaptic structural adjustments (Figure 2B & C, blue data; see
146 also Figure 1 – supplement 1). While bouton number positively correlates with increases in
147 motoneuron activity, quantification of synapse number, measured by quantification of active
148 zones, describes a more complex relationship. As previously published, a moderate increase
149 in activity (rearing larvae at 29°C) causes more boutons and also more active zones to be
150 formed, thus potentiating transmission at the NMJ (Sigrist et al., 2003). In contrast, further
151 increases in network activity, as effected by rearing larvae at 32°C, or cell-specific dTrpA1-
152 mediated motoneuron activation led to progressive active zone reductions, consistent with a
153 homeostatic response (Figure 2D, E).

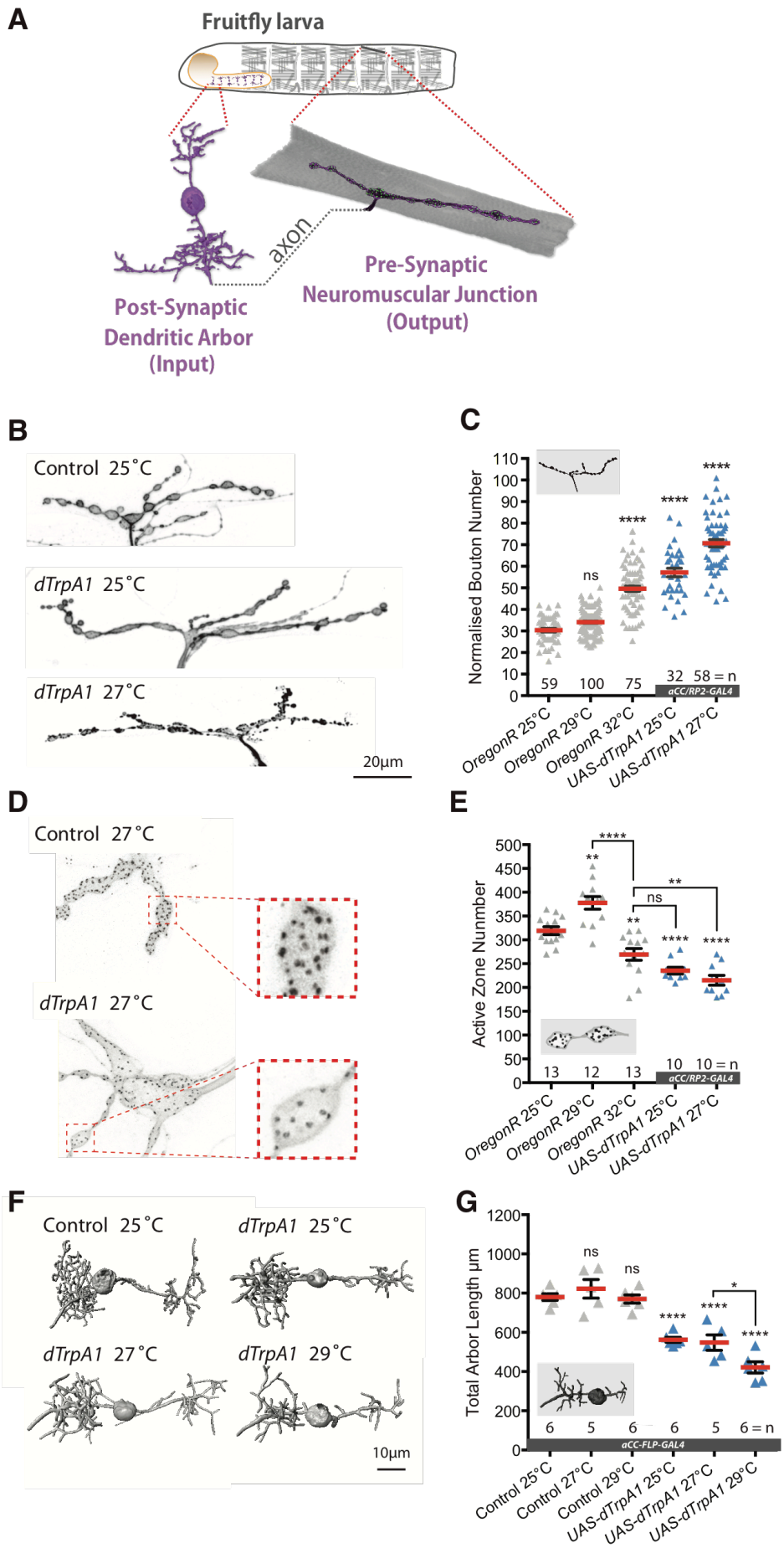
A
Fruitfly larva
axon
Post-Synaptic
Dendritic Arbor
(Input)
Pre-Synaptic
Neuromuscular Junction
(Output)
B
Control 25˚C
dTrpA1 25˚C
dTrpA1 27˚C
20µm
C
Normalised Bouton Number
ns
****
59 100 75 32 58 = n
aCC/RP2-GAL4
OregonR 25°C
OregonR 29°C
OregonR 32°C
UAS-dTrpA1 25°C
UAS-dTrpA1 27°C
D
Control 27˚C
dTrpA1 27˚C
E
Active Zone Nunmber
**
ns
****
13 12 13 10 10 = n
aCC/RP2-GAL4
OregonR 25°C
OregonR 29°C
OregonR 32°C
UAS-dTrpA1 25°C
UAS-dTrpA1 27°C
F
Control 25˚C
dTrpA1 25˚C
dTrpA1 27˚C
dTrpA1 29˚C
10µm
G
Total Arbor Length µm
ns
*
****
6 5 6 6 5 6 = n
aCC-FLP-GAL4
Control 25°C
Control 27°C
Control 29°C
UAS-dTrpA1 25°C
UAS-dTrpA1 27°C
UAS-dTrpA1 29°C

Figure 2: Adaptive structural synaptic plasticity at motorneuron input and output terminals in response to increased neuronal activity. (**A**) Graphical illustration of a stereotypical larval motorneuron (MN), adapted from (Kohsaka et al., 2012). Pre-motor interneurons make synaptic connections with the MN dendritic arbor (input) in the larval ventral nerve cord (equivalent of mammalian spinal cord). The MN extends an axonal projection into the periphery where it connects with a target muscle via an NMJ, characterized by varicose swellings (boutons) each containing multiple individual neurotransmitter release sites (active zones). (**B** and **C**) Representative images of muscle DA1[muscle 1] NMJs from 3rd instar larvae (100hrs ALH). Dot-plot quantification shows NMJ bouton number increases in response to systemic and cell-specific activity increases. (**D** and **E**) Active zone number increases following low-level over-activation (29°C), but progressively reduces upon stronger over-activation. (**F** and **G**) Digital reconstructions and dot plots show that over-activation leads to reduced total dendritic arbor length of aCC motoneurons (24hrs ALH). '*aCC/RP2-GAL4*' expresses GAL4 in all, '*aCC-FLP-GAL4*' in single aCC and RP2 motoneurons (see Online Methods for details); 'Control' in (F + G) is *aCC-FLP-GAL4* alone. Mean +/- SEM, ANOVA, ns = not significant, *P<0.05, **P<0.01, ***P<0.001, ****P<0.0001, n = replicate number. Comparisons with control are directly above data points.

We then turned to look at the input arbor of the motoneuron, branched dendrites on which the pre-motor interneurons form connections (Baines et al., 1999; Schneider-Mizell et al., 2016; Zwart et al., 2013). Using a stochastic labeling strategy within a small subset of motoneurons (aCC-FLP-GAL4) (Ou et al., 2008), we selectively targeted GAL4 and dTrpA1 expression to individual aCC motoneurons. Following confocal imaging and digital reconstructions of the arbors (Evers et al., 2005; Schmitt et al., 2004), morphometric analysis revealed that the size of the postsynaptic dendritic arbor decreased with rising levels of temperature-gated dTrpA1 activity (Figure 2F, G). Because in these motoneurons dendritic length correlates with input synapse number and synaptic drive (Tripodi et al.,

165 2008; Zwart et al., 2013), we interpret this structural adjustment of the dendrites as
166 homeostatic.
167 Thus, while a moderate increase in neuronal activity can lead to potentiation of the
168 presynaptic motoneuron terminal by increasing bouton and synapse number (Ataman et al.,
169 2008; Piccioli and Littleton, 2014; Sigrist et al., 2003), stronger over-activation leads to
170 structural adjustments at both input and output terminals of the motorneuron that we
171 interpret as compensatory; smaller dendritic arbors being associated with less synaptic drive
172 (Zwart et al., 2013) and fewer presynaptic release sites at the NMJ reducing transmission to
173 the muscle.
174

175 **Activity generated ROS regulate structural plasticity at synaptic terminals**

176 Because neural activity is energetically demanding (Attwell and Laughlin, 2001; Hallermann
177 et al., 2012; Zhu et al., 2012) we wondered whether neurons might monitor activity levels
178 through metabolic signals. Others previously reported that neuronal over-activation *in vitro*
179 can lead to a decrease in the ATP:ADP ratio (Tantama et al., 2013) and an increase in
180 mitochondrial ROS (Hongpaisan et al., 2004). Moreover, at the *Drosophila* NMJ oxidative
181 stress has been shown to regulate NMJ structure (Milton et al., 2011). To ask whether ROS
182 signaling might be associated with activity-dependent synaptic terminal growth, we
183 expressed the mitochondrion-targeted ratiometric ROS reporter *UAS-mito-roGFP2-Orp1* in
184 aCC and RP2 motoneurons (Gutscher et al., 2009). This reports a titratable neuronal
185 activity-dependent increase in mitochondrial ROS (Figure 3A).
186 We therefore hypothesized that mitochondrially derived ROS might provide a
187 readout of neuronal activity and regulate synaptic structural plasticity. To test this
188 hypothesis, we selectively increased neuronal activity in the aCC and RP2 motoneurons
189 while at the same time over-expressing the ROS scavenging enzymes Superoxide Dismutase
190 2 (SOD2, which catalyses O_2^- to H_2O_2 reduction) or Catalase (H_2O_2 into H_2O and O_2).
191 Catalase co-expression significantly counteracted dTrpA1 activity-induced bouton addition
192 at the NMJ (Figure 3B) and rescued motoneuron dendritic arbor size in the CNS (Figure 3C).

193 SOD2 co-expression on the other hand enhanced dTrpA1-mediated NMJ elaboration,
194 presumably by potentiating conversion of neuronal activity-induced O_2^- into H_2O_2 (Figure
195 3B). We then confirmed that ROS are also sufficient to invoke structural plasticity in the
196 absence of neuronal activity manipulation through cell-specific RNAi knock down of SOD1,
197 SOD2 and Catalase (Figure 3B). All of these manipulations led to NMJ growth phenotypes
198 with increased bouton number that are similar to those produced by neuronal over-
199 activation. Based on these results, we implicate ROS, specifically H_2O_2, in the observed
200 activity-dependent structural plasticity.

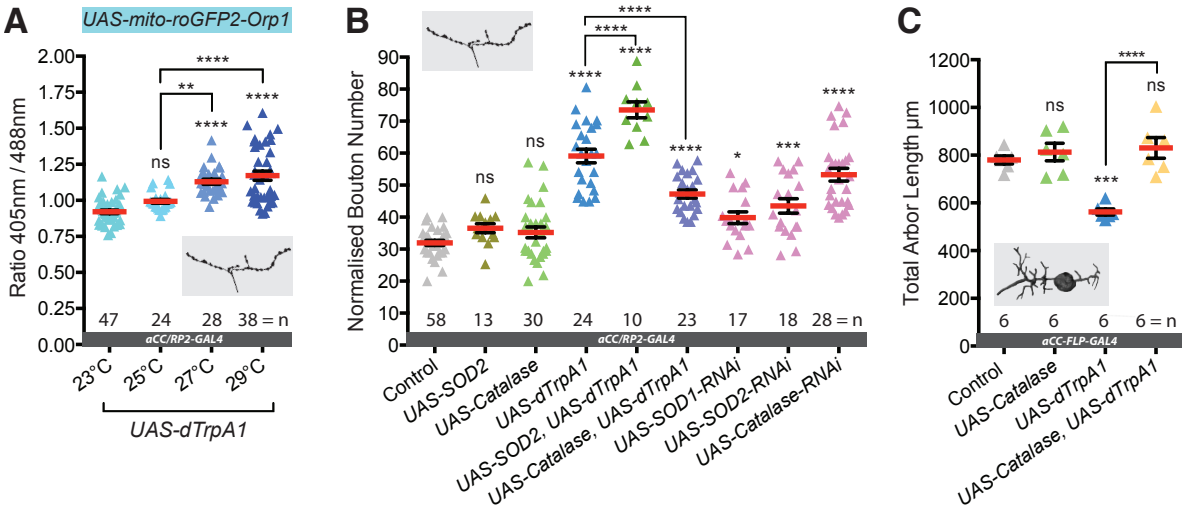

201

Figure 3: Neuronal activation leads to generation of synaptic ROS that regulate structural plasticity at input and output terminals. (**A**) Elevated neuronal activity increases mitochondrial ROS production at NMJs. Dot plots of mitochondrion-targeted ratiometric H_2O_2 sensor (*UAS-mito-roGFP2-Orp1* (Gutscher et al., 2009)) in wandering 3rd instar larval NMJs (100hrs ALH) at 23˚C (control, dTrpA1 inactive), 25˚C (moderate activity, ~10Hz), 27˚C (strong activity, ~20Hz) and 29˚C (very strong excitation, ~40Hz). (**B**) Bouton number at the NMJ is increased by *UAS-dTrpA1*-mediated over-activation. This is exacerbated by co-expression of *UAS-SOD2* (converts O_2^- to H_2O_2) and rescued by the H_2O_2 scavenger *UAS-Catalase*. Cell-specific ROS elevation by scavenger knockdown is sufficient to induce NMJ elaboration. *aCC/RP2-GAL4*, 'Control' is *aCC/RP2-GAL4* alone. (**C**) Total dendritic arbor length is reduced by single cell over-activation, but rescued by co-expression of the H_2O_2 scavenger *UAS-Catalase* (aCC motoneurons, 24hr ALH). *aCC-FLP-GAL4*, 'Control' is *aCC-FLP-GAL4* alone. Larvae reared at 25°C. Mean +/- SEM, ANOVA, ns = not significant, *P<0.05, **P<0.01, ***P<0.001, ****P<0.0001, n = replicate number.

202

203

204

205

206 **DJ-1ß acts as a ROS sensor in neurons**

207 We then asked how neurons might sense changes in activity-induced ROS levels. ROS are
208 known to post-transcriptionally modify many different proteins, principally on cysteine
209 residues, including transcription factors, cell adhesion molecules and phosphatases (for
210 review see (Milton and Sweeney, 2012)). Following a literature review, we focused on DJ-1ß,
211 the fly ortholog of DJ-1 (PARK7), as a candidate ROS sensor. *DJ-1* codes for a highly
212 conserved, ubiquitously expressed redox-sensitive protein, that protects against oxidative
213 stress and regulates mitochondrial function (Ariga et al., 2013; Nagakubo et al., 1997). A
214 mutant allele is also linked to a rare form of familial Parkinsonism (Bonifati et al., 2003).
215 *DJ-1* null mutant adult flies had been reported to be more sensitive to oxidative stress,
216 induced by exposure to paraquat and H_2O_2 (Meulener et al., 2005). We found that *DJ-1β* null
217 mutant (*DJ-1β*$^{\Delta 93}$) larvae develop normally and have structurally normal NMJs (Figure 4A
218 and Figure 4-supplement 1). What is more, systemic loss of DJ-1ß (*DJ-1β*$^{\Delta 93}$ null mutants)
219 completely rescues NMJ bouton addition phenotypes normally caused by pharmacologically
220 induced oxidative stress (Milton et al., 2011) (Figure 4A). Loss of DJ-1ß also significantly
221 rescues NMJ bouton phenotypes induced by cell type-specific expression of the ROS
222 generator Duox or dTrpA1-mediated over-activation (Figure 4A). *DJ-1β*$^{\Delta 93}$ mutant larvae
223 failed to produce the presynaptic bouton and active zone addition characteristic of NMJ
224 potentiation as seen in controls following periods of temperature-stimulated (29°C)
225 increases in locomotor activity (Sigrist et al., 2003) (Figure 4 – supplement 2). Motoneuron-
226 targeted expression of a dominant-acting mutant form of DJ-1ß that is non-oxidizable at the
227 conserved cysteine 104 (DJ-1ß^{C104A}) abrogated dTrpA1 activity-mediated NMJ structural
228 adjustment, both with respect to bouton number (Figure 4A) and active zone number
229 (Figure 4B). Looking at structural plasticity of the postsynaptic dendritic arbor, we found
230 that halving the *DJ-1β* copy number (in *DJ-1β*$^{\Delta 93}$/+ heterozygotes) was sufficient to
231 significantly suppress dTrpA1-mediated reductions in dendritic arbor size (Figure 4C).

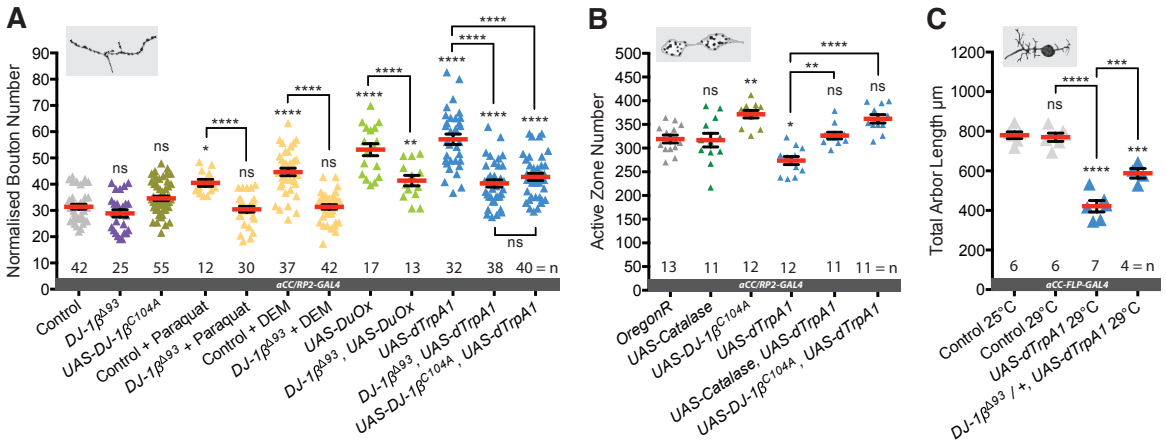

232

Figure 4: *DJ-1β* senses ROS and regulates activity-induced neural plasticity. (**A**) *DJ-1β* is required for ROS and neuronal activity-induced NMJ elaboration (100hrs ALH). Larvae reared at 25°C. (**B**) Cell-specific expression of *DJ-1β^{C104A}*, non-oxidizable on conserved cysteine C104, prevents activity-induced reduction of active zone number. *aCC/RP2-GAL4*, 'Control' is *aCC/RP2-GAL4* alone. Larvae reared at 25°C. (**C**) Activity-generated ROS sensing is dose sensitive. Removal of one copy of *DJ-1β* (in *DJ-1β^{Δ93} / +* heterozygotes) is sufficient to significantly rescue activity-induced reduction of total dendritic arbor length of motoneurons in 24hr ALH larvae. *aCC-FLP-GAL4*, 'Control' is *aCC-FLP-GAL4* alone.

233

234 In summary, these data show that DJ-1ß is necessary for sensing activity-induced
235 ROS and for implementing structural changes at both pre- and postsynaptic terminals in
236 response. At the presynaptic NMJ, DJ-1ß appears to be required in motoneurons for at least
237 two kinds of activity regulated structural plasticity: following mild over-activation, the
238 addition of both boutons and active zones, which are associated with potentiation (Sigrist et
239 al., 2003); and following stronger over-activation, reduction of active zone number, which
240 we interpret as an adaptive adjustment.

241

242

243

244 **Structural plasticity of synaptic terminals is required for homeostatic**
245 **adjustment of locomotor behavior**

246 We then asked whether this ROS - DJ-1ß mediated structural plasticity of synaptic terminal
247 growth was required for the homeostatic adjustments of crawling speed, which ensues after
248 prolonged over-activation. To answer this question, we targeted expression of the dominant
249 acting non-oxidizable DJ-1ß^{C104A} to motoneurons (and other glutamatergic cells, using
250 DvGlut-T2A-GAL4). We then tested the behavior of these animals for adjustment in
251 response to *chronic* temperature-induced elevation of motor network activity. Our previous
252 experiments showed that expression of non-oxidizable DJ-1ß^{C104A} in motoneurons does not
253 lead to abnormal bouton number or the decrease in active zone number normally caused by
254 over-activation (see Figures 4A & 4B). Expression of non-oxidizable DJ-1ß^{C104A} in
255 motoneurons per se did not alter larval crawling speed at the control temperature of 25°C.
256 However, when rearing these larvae at 32°C, which is associated with elevated motor
257 network activation, unlike controls they failed to homeostatically adjust toward the default
258 crawling speed set point (Figure 5). Consequently, such larvae reared at elevated
259 temperatures (29°C or 32°C) also responded less strongly than controls to acute temperature
260 downshifts (Figure 5). These data suggest that activity-induced neuronal plasticity,
261 implemented through the ROS sensor DJ-1ß, is necessary for activity-directed homeostatic
262 adjustment of larval locomotor behavior.

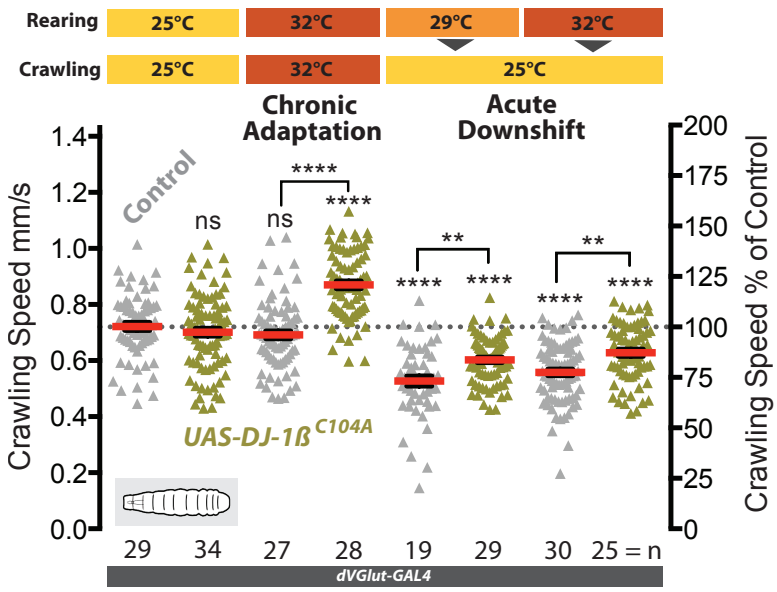

Figure 5: *DJ-1β* is required in motoneurons for behavioral plasticity in response to chronic locomotor over-activation. Larvae with expression of *UAS-DJ-1β^{C104A}* targeted to motoneurons (*dVGlut-GAL4*) are unable to adapt motor network output (crawling speed) to elevated rearing temperatures. Control is *dVGlut-GAL4* alone. Each data point represents crawling speed from an individual uninterrupted continuous forward crawl, n = specimen replicate number, up to 3 crawls assayed for each larva. Mean +/- SEM, ANOVA, ns = not significant, **P<0.01, ****P<0.0001, n = replicate number.

PTEN and PI3K are downstream effectors of the DJ-1ß ROS sensor

Next, we looked for downstream effector pathways responsible for implementing activity and ROS-dependent structural plasticity. DJ-1 is a known redox-regulated inhibitor of Phosphatase and Tensin homologue (PTEN) and thus a positive regulator of PI3Kinase signaling (R. H. Kim et al., 2005; Y.-C. Kim et al., 2009); and PI3Kinase is a known positive regulator of NMJ development (Jordán-Álvarez et al., 2012; Martín-Peña et al., 2006). To test whether DJ-1ß - PTEN interactions mediate ROS-dependent NMJ adjustments, we performed genetic interaction experiments in the context of a DEM (oxidative stress) dose-response curve (Figure 6A). Focusing on the NMJ, we found that in controls bouton number

274 increases linearly with exposure to increased DEM concentrations, peaking at 15mM DEM
275 (Figure 6A). Removing one copy of *DJ-1β* (*DJ-1β*$^{\Delta 93}$/+) was sufficient to suppress DEM-
276 induced increases in bouton number. In contrast, *PTEN*^{CO76}/+ heterozygous larvae showed
277 increased sensitivity to DEM, with a left-shifted dose response curve. Larvae heterozygous
278 for both *DJ-1β* and *PTEN* (*PTEN*^{CO76}/+; *DJ-1β*$^{\Delta 93}$/+) were more sensitive to DEM at higher
279 concentrations than *DJ-1β*$^{\Delta 93}$/+ heterozygotes. These genetic interactions agree with
280 previous studies (R. H. Kim et al., 2005) and complement biochemical data that showed
281 H_2O_2-oxidized DJ-1ß binds to and inhibits PTEN (Y.-C. Kim et al., 2009).

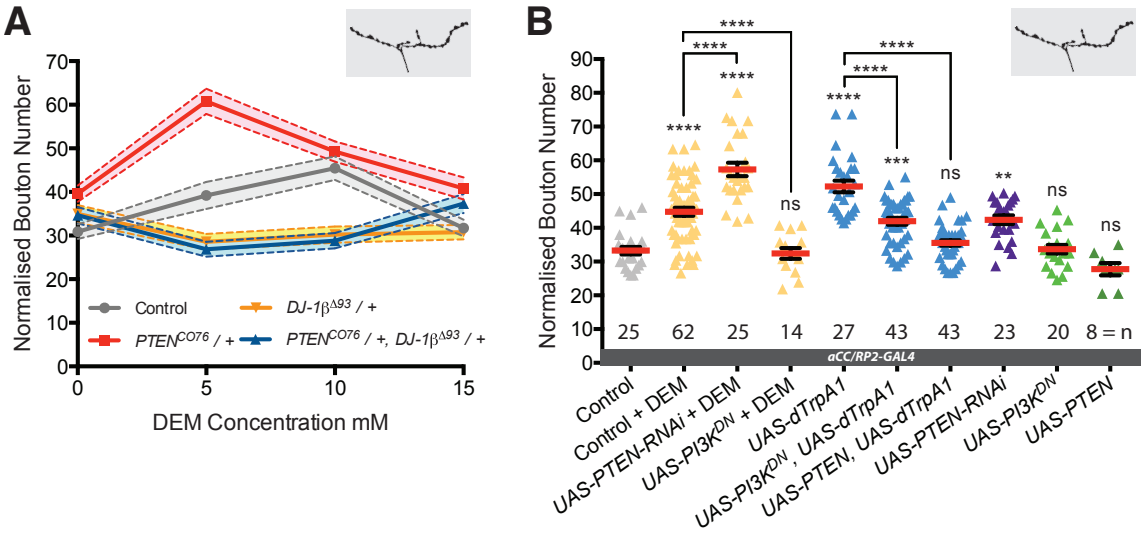

282

Figure 6: *DJ-1β* signals via PTEN and PI3Kinase to regulate ROS and activity-induced NMJ elaboration. (**A**) *DJ-1β* and PTEN genetically interact to regulate systemic ROS-induced NMJ elaboration. NMJ bouton number varies with ROS (DEM) levels (grey data). Removal of one copy of *PTEN* sensitizes (red) while heterozygosity for *DJ-1β* desensitizes NMJs to ROS levels (yellow), partially restored in double heterozygotes (blue). Dashed boundaries indicate 95 % confidence intervals (n≥38). (**B**) Systemic ROS and activity-induced NMJ structural adjustments require PTEN and PI3Kinase signaling. Over-expression of the PI3Kinase antagonist PTEN or a dominant negative PI3Kinase form abrogates activity-induced NMJ elaboration. *aCC/RP2-GAL4*, 'Control' is *aCC/RP2-GAL4* alone. Mean +/- SEM, ANOVA, ns = not significant, **P<0.01, ***P<0.001, ****P<0.0001, n = replicate number.

283 To further test specificity, we manipulated PTEN and PI3Kinase activities in single
284 cells. Targeted knock-down of PTEN in motoneurons sensitized these neurons to ROS,
285 exacerbating the DEM-induced bouton addition phenotype (Figure 6B). In contrast, over-
286 expression of PTEN or mis-expression of a dominant negative form of PI3Kinase
287 significantly reduced NMJ elaboration normally caused by DEM exposure or dTrpA1-
288 mediated neuronal activity increase (Figure 6B). Together these interactions suggest that
289 PTEN and PI3Kinase act downstream of DJ-1ß and neural activity-generated ROS; and that
290 oxidation of DJ-1ß, through PTEN inhibition, facilitates a rise in PI3Kinase / PIP_3 signaling,
291 which in turn mediates at least part of the structural synaptic terminal plasticity (Figure 7).

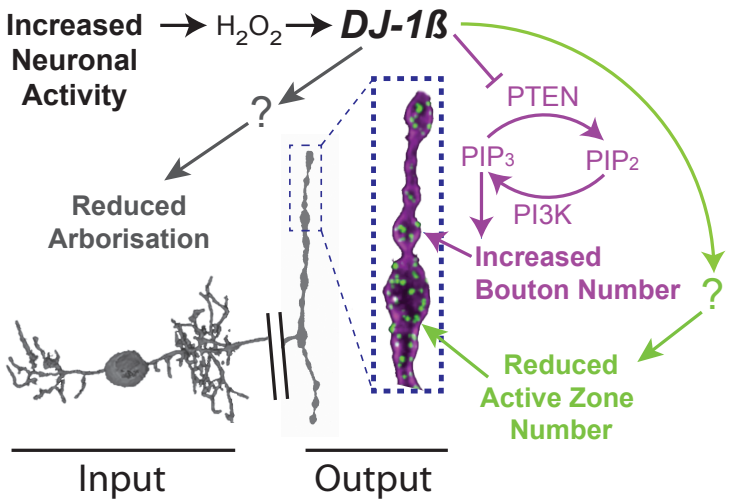

292

Figure 7: Model summary. *DJ-1β* is a redox signaling hub that coordinates structural synaptic plasticity at motoneuron synaptic input and output terminals. Activity-induced ROS oxidize *DJ-1β*, leading to PTEN inhibition and thus to a gain in PI3Kinase signaling, which regulates activity-induced NMJ elaboration of boutons and active zones. At higher activity/ROS thresholds additional, yet to be defined, pathways downstream of *DJ-1β* are activated, implementing adaptive reductions of active zones at the NMJ and dendritic arbor length in the CNS.

293

294

295

296 # Discussion

297 Our aim was to study mechanisms of structural plasticity in relation to neuronal activity in a
298 motor network. To do so we used as a model the *Drosophila* larva and focused on major
299 effectors of motor circuit output: motoneurons, their dendrites in the CNS and presynaptic
300 terminals at peripheral neuromuscular junctions. We have identified a novel pathway by
301 which these neurons sense changes in activity through measuring increases in activity-
302 generated ROS, which act as second messengers for structural adjustments at both dendritic
303 input and presynaptic output terminals. Our data further suggest that this activity-regulated
304 structural plasticity is instrumental for the homeostatic adjustment of larval locomotor
305 network activity and thus crawling behavior.

306

307 ## Homeostatic adjustment of the motor network allows animals to maintain a
308 dynamic range of crawling speed

309 To investigate forms and mechanisms of structural plasticity that neurons undertake while
310 adapting to altered activity levels, we took advantage of *Drosophila* motor network activity
311 being readily manipulated through changes in ambient temperature. We found that while
312 acute increases in ambient temperature from 25°C to 29°C or above quickly push larvae to
313 their maximum crawling speed (approx. 0.8mm/sec), prolonged exposure leads to the
314 network adjusting homeostatically toward a default crawling speed (approx. 0.65mm/sec)
315 (Figure 1A). This adaptation might overall be energetically more favorable, and it allows
316 larvae to stay within their dynamic range of behavioral responses to relative changes
317 regardless of absolute ambient temperature.

318 Cell type-specific over-activation of the glutamatergic motoneurons (via dTrpA1)
319 largely recapitulated the larval crawling phenotypes otherwise generated by systemic motor
320 network overactivation. Conversely, blockade of activity-induced structural adjustment
321 (through mis-expression of non-oxidisable DJ-1ß^{C104A}) in the glutamatergic motoneurons
322 significantly blocked homeostatic locomotor network adjustment to higher ambient

323 temperatures (Figure 1B). The importance of the motoneurons in shaping much of the
324 adaptive behavioral response is perhaps to be expected, since their dendrites are the final
325 integrators on which all pre-motor inputs converge (Fushiki et al., 2016; Itakura et al., 2015;
326 Kohsaka et al., 2014; Schneider-Mizell et al., 2016; Zwart et al., 2016). Systemic
327 manipulations produce stronger behavioral phenotypes than those targeted to the
328 glutamatergic neurons, suggesting, as would be expected, that other cells within the
329 locomotor network are also subject to activity-regulated homeostatic plasticity (Figure 5).
330 Interestingly, a recent study, which modeled different forms of plasticity in this motor
331 network, concluded that during its development homeostatic mechanisms are better placed
332 in achieving the formation of a stable balanced network producing robust activity patterns
333 than Hebbian alternatives (Gjorgjieva et al., 2016).
334

335 **Structural adjustment coordination between pre- and postsynaptic terminals**

336 Working with identified motoneurons we attempted to take an integrated view by relating
337 structural plasticity across its pre-synaptic and dendritic terminals. At the presynaptic NMJ
338 low-level increases of activity lead to potentiation, associated with increased numbers of
339 active zones, elevated levels of the Brp/CAST/ELKS family active zone protein Bruchpilot
340 (Brp) and the addition of boutons, varicose swellings containing multiple active zones (Cho
341 et al., 2015; Sigrist et al., 2003; Vasin et al., 2014; Weyhersmüller et al., 2011).It is known
342 that changes to the composition of the active zone cytomatrix (Davydova et al., 2014;
343 Lazarevic et al., 2011; Matz et al., 2010) such as elevation of Brp levels can further aid
344 transmission by increasing release probability (Peled et al., 2014; Weyhersmüller et al.,
345 2011).

346 Strong over-activation, in contrast, though triggering further addition of boutons,
347 leads to overall reductions in active zone number at the NMJ, which correlate with the
348 severity of over-activation (Figure 2D, E). This parallels observations in the adult *Drosophila*
349 visual system where increased activation also triggers a reduction of Brp levels in
350 photoreceptor terminals (Sugie et al., 2015). We interpret this negative correlation between

351 the degree of over-activation and the reduction in active zone number, and potentially Brp
352 content, as a compensatory response. In agreement, blocking activity-induced structural
353 adjustment in the motoneurons abrogates behavioral adaptation to prolonged over-
354 activation (Figure 5). Whether increased numbers of smaller boutons forms part of an
355 adaptive response to over-activation or is anticipatory of future synapse strengthening
356 remains to be established.

357 The input terminal of the neuron, the dendritic arbor in the CNS, responds to over-
358 activation with corresponding reductions in dendritic length, which we previously found to
359 correlate with reducing both input synapses and synaptic drive. We therefore interpret this
360 activity driven structural adjustment of the dendrites also as compensatory (Tripodi et al.,
361 2008; Zwart et al., 2013). In summary, we found that above threshold over-activation
362 regimes lead to structural adaptive adjustments at both the postsynaptic input and
363 presynaptic output terminals. We do not yet know whether these are regulated locally or
364 globally coordinated by transcriptional changes; though at least for the presynaptic NMJ
365 activity and ROS mediated structural changes have been reported as dependent on
366 immediate early genes (AP-1) (Milton et al., 2011; Sanyal et al., 2002). Given the available
367 evidence we would expect these structural adjustments to be linked to, and potentially
368 preceded by compensatory changes in neuronal excitability (Baines et al., 2001; Davis, 2006;
369 Davis et al., 1996; 1998; Driscoll et al., 2013; Frank et al., 2006; 2009; Gaviño et al., 2015;
370 Giachello and Baines, 2016; Lin et al., 2012; Mee et al., 2004; Müller and Davis, 2012;
371 O'Leary et al., 2013; Prinz, 2006; Prinz et al., 2004; Wang et al., 2014; Younger et al., 2013).
372

373 **ROS and redox sensitive DJ-1ß provide a readout of neuronal activity**

374 Neurons have cell type-specific set points of average firing ranges to which they return
375 following activity perturbations using a variety of homeostatic plasticity mechanisms
376 (Hengen et al., 2016; 2013; Keck et al., 2017; 2013). The mechanisms that determine the
377 homeostatic set point and allow neurons to sense when their activity deviates from such a set
378 point are not yet known. Intracellular concentrations of calcium correlate with neuronal

379 activity (Hardingham et al., 2001), making this versatile second messenger a prime
380 candidate for providing a readout of activity and for regulating homeostatic plasticity
381 (O'Leary et al., 2014). In this study we asked whether metabolically associated signals, such
382 as ROS, might also be involved, as these could provide a proxy measure of neuronal activity
383 (Attwell and Laughlin, 2001; Zhu et al., 2012). Over-activation measurably impacts on the
384 ADP:ATP ratio (Tantama et al., 2013) and generates mitochondrial ROS. These can
385 modulate calcium dependent signaling pathways, such as CamKII (Hongpaisan et al., 2004),
386 and potentially also other ROS sensitive pathway components including IP_3 and Ryanodine
387 receptor channels or the protein phosphatase Calcineurin (Hidalgo and Arias-Cavieres,
388 2016). We found that a mitochondrially targeted ROS sensor (Albrecht et al., 2011; Gutscher
389 et al., 2009) became progressively oxidized with increasing levels of neuronal over-activation
390 (Figure 3A). Moreover, ROS were necessary for (and their elevation was also sufficient to
391 mimic) implementing activity-induced structural plasticity at synaptic terminals (Figure 3B,
392 C). Thus, our data show that ROS, particularly H_2O_2, are both necessary and sufficient for
393 activity regulated structural plasticity. The source of the activity-generated ROS appears to
394 be mitochondrial, potentially generated as a byproduct of increased ATP metabolism or
395 triggered by mitochondrial calcium influx (Peng and Jou, 2010). However, other ROS
396 generating systems could also be involved, notably NADPH oxidases, some of which are
397 regulated by calcium (Kishida et al., 2006; 2005; Serrano et al., 2003; Tejada-Simon et al.,
398 2005).

399 We discovered that in neurons the highly conserved protein DJ-1ß is critical for
400 responding to activity-generated ROS with structural changes to synaptic terminals (Figure
401 4A, B, C), and propose that in neurons DJ-1ß acts as a redox sensor for activity-generated
402 ROS. In agreement with this idea, DJ-1ß has been shown to be oxidized at the conserved
403 cysteine residue C106 (C104 in *Drosophila*) by H_2O_2. Oxidation of DJ-1 leads to changes in
404 DJ-1 function, including translocation from the cytoplasm to the mitochondrial matrix,
405 which aids with protection against oxidative damage (Blackinton et al., 2009; Canet-Avilés
406 and Wilson, 2004; Waak et al., 2009) and maintenance of ATP levels (Calì et al., 2015). We

407 found that motoneurons are potently sensitive to DJ-1ß dosage with regard to their response
408 to altered activity and ROS levels, and expression of mutant DJ-1ß^{C104A} in motoneurons
409 blocks their structural plasticity response to DEM and over-activation. These observations
410 suggest that DJ-1ß forms a critical part of the ROS sensing mechanism in neurons. It is
411 therefore conceivable that different sensitivities to neuronal activity could in part be
412 determined by cell type-specific levels of DJ-1ß and associated reducing mechanisms.
413

414 **DJ-1ß downstream pathways implement activity-regulated plasticity**

415 Our data suggest that DJ-1ß forms part of a signaling hub required for at least two opposing
416 types of structural plasticity that seem to be implemented by distinct pathways: potentiation
417 in response to low-level increases in neuronal activation versus compensatory changes
418 following stronger over-activation. In this study we demonstrated that DJ-1ß mediates the
419 former by activation of PI3Kinase signaling following redox-regulated binding and inhibition
420 of PTEN (Figure 4A) (R. H. Kim et al., 2005; Y.-C. Kim et al., 2009). PTEN and PI3Kinase
421 are both intermediates of metabolic signaling pathways and regulators of synaptic terminal
422 growth (Jordán-Álvarez et al., 2012; Martín-Peña et al., 2006). While activity and ROS levels
423 correlate positively with PTEN/PI3Kinase mediated bouton addition at the NMJ, active zone
424 number regulation is more nuanced; at a higher activity threshold other, yet to be identified
425 effector pathways appear to be activated that reduce presynaptic active zone number (Figure
426 2D, E). Because this too is dependent on DJ-1ß we would expect this pathway also to be
427 regulated by activity-generated ROS. Equally unresolved is the question of how postsynaptic
428 dendritic arbor size in the CNS is regulated. PTEN/PI3Kinase signaling is an unlikely
429 candidate as this normally stimulates neuronal and dendritic growth (Brierley et al., 2009).
430

431 **ROS as gatekeepers of activity-dependent synaptic structural plasticity**

432 Synaptic plasticity is regulated by a number of signaling pathways, including Wnts (Budnik
433 and Salinas, 2011), BMPs (Bayat et al., 2011; Berke et al., 2013), as well as PKA, CREB and
434 AP-1 (Cho et al., 2015; Davis, 2006; Davis et al., 1998; 1996; Davis and Müller, 2015; S. M.

435 Kim et al., 2009; Koles and Budnik, 2012; Osses and Henriquez, 2014; Sanyal et al., 2002;
436 2003; Sulkowski et al., 2014; Walker et al., 2013). Here we demonstrated a requirement for
437 ROS for activity-dependent structural plasticity at the *Drosophila* NMJ and motoneuron
438 dendrites. Like BMP (Berke et al., 2013) and AP-1 (Milton et al., 2011; Sanyal et al., 2002)
439 ROS have the potential to act as gatekeepers of neuronal plasticity. If acting as a parallel
440 stimulus, ROS signaling at the synapse could be synergistic with other plasticity pathways,
441 which could help overcome issues with biological noise and increase the fidelity of cellular
442 decision making. Alternatively, ROS might deliver requisite post-translational redox
443 modifications to components of other signaling pathways. In support of the latter, ROS
444 regulate by redox modification the activity of the immediate early genes Jun and Fos, which
445 are required for LTP in vertebrates and in *Drosophila* for activity-dependent plasticity of
446 motoneurons, both at the NMJ and central dendrites (Hartwig et al., 2008; Jindra et al.,
447 2004; Loebrich and Nedivi, 2009; Milton et al., 2011; Milton and Sweeney, 2012; Sanyal et
448 al., 2002). ROS modulation of BMP signaling has recently been shown in cultured
449 sympathetic neurons (Chandrasekaran et al., 2015) and of Wnt pathways in non-neuronal
450 cells (Funato et al., 2006; Love et al., 2013; Rharass et al., 2014).
451 Although we focused exclusively on structural plasticity in the *Drosophila* larva,
452 current evidence suggests synaptic ROS signaling is a conserved and central feature of
453 communication in the nervous system. Several studies have demonstrated a requirement for
454 ROS for Long Term Potentiation (Huddleston et al., 2008; Kamsler and Segal, 2003b;
455 2003a; Klann, 1998; Knapp and Klann, 2002; Lee et al., 2010) and also correlated defects in
456 learning with altered ROS signaling (Kishida et al., 2006). The underlying cellular and
457 molecular mechanisms though are far from clear, probably because of the complexity of ROS
458 signaling and because of the large number of potential redox sensitive targets. For example,
459 components of the presynaptic release machinery, notably SNAP25, are thought to be
460 modulated by ROS (Giniatullin et al., 2006). Here, we identified DJ-1ß as a ROS sensor in
461 neurons whose interactions with the PTEN/PI3Kinase synaptic growth pathway are
462 governed by redox regulation. This represents a novel mechanism by which ROS, potentially

generated as metabolic byproducts, are used to tune connectivity and communication within the nervous system through modifications of neuronal structure. Since ROS can diffuse through membranes these signals have the potential to act non-autonomously, possibly across synaptic partners. Our findings shine a new light on ROS which, when dysregulated with age or under neurodegenerative conditions, might interfere with neuronal adaptive adjustments and thus contribute to network malfunction and synapse loss.

Competing interests: The authors declare that no competing interests exist.

Author Contributions:

M.O., M.F.Z., S.T.S. & M.L. devised the project. M.O. performed most experiments and analyses. P.B., A.M., M.F.Z. & K.M. generated specimens and dendrite data on activity dependent dendrite growth. A.M. carried out experiments and analysis involving ROS measurements. R.J.H.W. processed specimens for TEM imaging and analysed TEM data. M.O. & M.L. co-wrote the manuscript and S.T.S. & M.L. co-supervised the project.

Acknowledgements:

We would like to thank Nancy Bonini, Tobias Dick, Jörg Grosshans, Karen Hibbard, Fanis Missirlis, Barret Pfeiffer and Alex Whitworth for generous fly stock and reagent donations, Other fly stocks were obtained from the Bloomington Stock Center. The monoclonal antibodies nc82 (anti-Bruchpilot), developed by E. Buchner and colleagues, was obtained from the Developmental Studies Hybridoma Bank, created by the NICHD of the NIH and maintained at The University of Iowa, Department of Biology. We thank Akinao Nose and Hiroshi Kohsaka for kindly sharing figure graphics, Benjamin Risse for his generous support with setting up a FIM Tracker and Matthew Wayland for his generous support with data analysis and imaging. We would also like to thank Jimena Berni, Alex Whitworth and members of the Landgraf lab for valuable comments on the manuscript. This work was supported by BBSRC research grants (BB/IO1179X/1, BB/M002934/1) to ML and

492 (BB/I012273/1, BB/M002322/1) to STS. This work benefited from facilities supported by a
493 Wellcome Trust Equipment Grant (WT079204) and contributions by the Sir Isaac Newton
494 Trust in Cambridge.

495

496 ## Materials and Methods

497

498 **Fly Strains and Husbandry.** Wild-type and transgenic strains were maintained on
499 standard yeast–agar–cornmeal medium at 25 °C. The following fly strains were used:
500 *OregonR* and *PTEN*^{CO76} (Bloomington Stock Center, Indiana University), *UAS-dTrpA1*
501 (Hamada et al., 2008), *UAS-SOD2* (Missirlis et al., 2003), *UAS-Catalase* (Missirlis et al.,
502 2001), *UAS-Duox* (Ha, 2005), *DJ-1β*$^{\Delta 93}$ (Meulener et al., 2005), *UAS-DJ-1β*^{C104A} (Meulener
503 et al., 2006), UAS-RNAi lines targeting *SOD1*, *SOD2*, *Catalase* and *PTEN* (KK collection,
504 Vienna Drosophila Resource Centre) (Dietzl et al., 2007), *UAS-PI3K*^{DN} (Leevers et al.,
505 1996), *UAS-PTEN* (Gao et al., 2000). The following two GAL4 expression lines were used to
506 target GAL4 to the aCC and RP2 motoneurons: *aCC-FLP-GAL4* (*eveRN2-Flippase, UAS-*
507 *myr::mRFP1, UAS-Flp, tubulin84B-FRT-CD2-FRT-GAL4*) (Roy et al., 2007) expresses
508 GAL4 stochastically in single aCC and RP2 motoneurons allowing the imaging of aCC
509 neurons in isolation, as required for dendritic arbor resolution and reconstruction.
510 *aCC/RP2-GAL4* (*eveRN2-GAL4* (Fujioka et al., 2003)*, UAS-myr-mRFP1, UAS-Flp,*
511 *tubulin84B-FRT-CD2-FRT-GAL4; RRaGAL4, 20xUAS-6XmCherry::HA* (Shearin et al.,
512 2014)) was used for NMJ analysis as it expresses GAL4 in every aCC and RP2 motoneuron.
513 *eveRN2-GAL4* expression is restricted to the embryo and FLPase-gated *tubulin84B-FRT-*
514 *CD2-FRT-GAL4* maintains GAL4 expression at high levels during larval stages.

515

516 ### Dissection and Immunocytochemistry

517 **1st Instar Ventral Nerve Cord (VNC).** Flies were allowed to lay eggs on apple juice-based
518 agar medium for 24 hrs at 25°C. Embryos were dechorionated using bleach (3.5 minutes

519 room temperature) then incubated (25°C) in pre-warmed Sorensen's saline (pH 7.2, 0.075
520 M) whilst adhered to a petri dish. Hatched larvae (floating) were recovered hourly and
521 transferred to pre-warmed apple-juice agar plates supplemented with yeast paste. Larvae
522 were allowed to develop for a further 24 hrs (24 hrs after larval hatching, ALH) at 25°C, 27°C
523 or 29°C prior to dissection in Sorensen's saline. A fine hypodermic needle (30 1/2 G;
524 Microlance) was used as a scalpel to cut off the anterior end of each larva, allowing gut, fat
525 body, and trachea to be removed. The ventral nerve chord and brain lobes, extruded with
526 viscera upon decapitation, were dissected out and transferred to a cover glass coated with
527 poly-L-lysine (Sigma-Aldrich), positioned dorsal side up in Sorensen's saline. A clean cover
528 glass was placed on top of the preparation, with strips of double-sided sticky tape as spacers
529 positioned along the edges.
530
531 **Wandering 3rd Instar.** Flies were allowed to lay eggs on apple-juice agar based medium
532 overnight at 25°C, larvae were then incubated at 25°C or 27°C until the late wandering 3rd
533 instar stage. Larvae were reared on yeast paste colored with Bromophenol Blue sodium salt
534 (Sigma-Aldrich) to allow visualization of gut-clearance, an indicator of the late wandering 3rd
535 instar stage. For Di-ethylmaleate (DEM) (Sigma-Aldrich) and paraquat (Sigma-Aldrich)
536 feeding, yeast paste was made using a 5 mM – 15 mM aqueous solution. Larvae were 'fillet'
537 dissected in Sorensen's saline and fixed for 15 minutes at room temperature in 4%
538 formaldehyde (in Sorenson's saline). Specimens were then washed and stained in Sorensen's
539 saline containing 0.3% Triton X-100 (Sigma-Aldrich) using the following primary and
540 secondary antibodies; Goat-anti-HRP Alexa Fluor 488 (1:400) or Goat-anti-HRP Alexa Fluor
541 594 (1:400) (Jackson ImmunoResearch Cat. Nos. 123-455-021 or 123-585-021), Rabbit-
542 anti-DsRed (1:1200) (ClonTech Cat. No. 632496), Donkey-anti-Rabbit CF568 (1:1200)
543 (Biotium Cat. No. 20098), Mouse-nc82 (1:100) (Developmental Studies Hybridoma Bank),
544 Donkey-anti-Mouse Alex Fluor 488 (1:600) (ThermoFisher Cat. No. A-21202) or Donkey-
545 anti-Mouse CF633 (1:300) (Biotium Cat. No. 20124) incubated overnight at 4°C or 2 hrs at

546 room temperature. Specimens were mounted in EverBrite mounting medium (Biotium Cat.
547 No. 23001).
548

549 **Image Acquisition and Analysis**

550 **1st Instar Ventral Nerve Cord (VNC).** Ventral nerve cords were pre-screened for
551 fluorescently labeled, isolated, aCC motoneurons using a Zeiss Axiophot compound
552 epifluorescence microscope and a Zeiss Plan-Neofluar 40x/0.75 N.A. objective lens. Suitable
553 VNCs were imaged immediately with a Yokagawa CSU-22 spinning disk confocal field
554 scanner mounted on an Olympus BX51WI microscope, using a 60×/1.2 N.A. Olympus water
555 immersion objective. Images were acquired with a voxel size of 0.2 × 0.2 × 0.3 μm using a
556 QuantEM cooled EMCCD camera (Photometrics), operated via MetaMorph software
557 (Molecular Devices). Dendritic trees were digitally reconstructed using Amira Resolve RT 4.1
558 (FEI), supplemented with a 3D reconstruction algorithm (Evers et al., 2005; Schmitt et al.,
559 2004), and images were processed using Amira (FEI) and ImageJ (National Institutes of
560 Health).
561

562 **Wandering 3rd Instar.** Dissected specimens were imaged using a Leica SP5 point-scanning
563 confocal, and a 63x/1.3 N.A. (Leica) glycerol immersion objective lens and LAS AF (Leica
564 Application Suite Advanced Fluorescence) software. Confocal images were processed using
565 ImageJ and Photoshop (Adobe). Bouton number of the NMJ on muscle DA1 [1] from
566 segments A3-A5 was determined by counting every distinct spherical varicosity along the
567 NMJ branch. DA1 muscles were imaged using a Zeiss Axiophot compound microscope and a
568 Zeiss Plan-Neofluar 10x/0.3 N.A. objective lens. Muscle surface area (MSA) was determined
569 by multiplying muscle length by width using ImageJ. In order to correct for subtle
570 differences in animal size (typically 5-10%) bouton number normalization was performed
571 using the following calculation: (mean control MSA / mean experimental MSA) x test bouton
572 number = normalized experimental bouton number.
573

574 **Ratiometric ROS Reporter.** *aCC/RP2-Gal4* was used to drive the expression of *UAS-*
575 *mito-roGFP2-Orp1* (Albrecht et al., 2011; Gutscher et al., 2009) in all aCC and RP2
576 motoneurons. Wandering third instar larvae were fillet dissected in PBS-NEM (137mM
577 NaCl, 2.7mM KCl, 10mM Na_2HPO_4, 1.8mM KH_2PO_4, 20mM N-ethylmaleimide (NEM), pH
578 7.4). Larval fillet preparations were incubated for 5 minutes in PBS-NEM then fixed for 8
579 minutes in 4% formaldehyde (in PBS-NEM). Specimens were washed three times in PBS-
580 NEM and then equilibrated in 70% glycerol. Specimens were mounted in glycerol and
581 imaged the same day. Imaging was performed on a Leica SP5 point-scanning confocal, using
582 a 63x/1.3 N.A. (Leica) glycerol immersion objective lens. The reporter was excited
583 sequentially at 405nm and 488nm (Albrecht et al., 2011) with emission detected at 500–
584 535nm. 16-bit images were acquired using Leica LAS AF software and processed using
585 ImageJ. Z-stack images were maximally projected and converted to 32-bit. To remove
586 fringing artefacts around bouton edges 488nm images were thresholded using the
587 'Intermodes' algorithm with values below threshold set to 'not a number', and ratio images
588 were created by dividing the 405nm image by the 488nm image pixel by pixel (Albrecht et
589 al., 2011). Regions of Interest were taken on the ratio image spanning the entire NMJ and
590 the mean value obtained from each NMJ was used for statistical analysis.
591
592 **Transmission Electron Microscopy.** Third instar wandering larvae were fillet
593 dissected in PBS and fixed overnight in 0.1M $NaPO_4$, pH 7.4, 1% glutaraldehyde, and 4%
594 formaldehyde, pH 7.3. Fixed specimens were washed 3× in 0.1M $NaPO_4$ before incubation
595 in OsO_4 (1% in 0.1M $NaPO_4$; 2hr). Preparations were washed 3× in distilled water,
596 incubated in 1% uranyl acetate, then washed again 3× in distilled water and dehydrated
597 through a graded ethanol series: 20% increments starting at 30% followed by two 100%
598 changes and then 2× 100% propylene oxide. Specimens were incubated in a graded series of
599 epon araldite resin (in propylene oxide): 25% increments culminating in 3× 100% changes.
600 Individual muscles were then dissected and transferred into embedding molds, followed by
601 polymerization at 60°C for 48 hrs. Resin mounted specimens were sectioned (60–70 nm)

602 using glass knives upon a microtome (Ultracut UCT; Leica). Sections were placed onto
603 grids, incubated in uranyl acetate (50% in ethanol), washed in distilled water and incubated
604 in lead citrate. Sections were imaged using a transmission electron microscope (TECNAI 12
605 G^2; FEI) with a camera (Soft Imaging Solutions MegaView; Olympus) and Tecnai user
606 interface v2.1.8 and analySIS v3.2 (Soft Imaging Systems).
607

608 **Behavior – larval crawling analysis**

609 To record larval crawling, mid-3rd instar larvae (72hrs ALH) were briefly rinsed in water to
610 remove any food and yeast residues, then up to 12 larvae were placed into a 24cm x 24cm
611 arena of 0.8% agar in water, poured to 5 mm thickness. Crawling behavior was recorded in a
612 temperature and humidity controlled incubator at temperatures ranging from 25-32°C, as
613 indicated for each experiment. Larvae were allowed to acclimatise for 5 minutes, then
614 recorded for 15 minutes under infrared LED illumination (intensity from 14.33 nW/mm^2 in
615 the edge to 9.12 nW/mm^2 in the center), using frustrated total internal reflection using a
616 modified FIM tracker (Milton et al., 2011; Risse et al., 2013) https://www.uni-
617 muenster.de/PRIA/en/FIM/index.html. Larvae were recorded with a Basler acA2040-
618 180km CMOS camera using Pylon and StreamPix software, mounted with a 16mm KOWA
619 IJM3sHC.SW VIS-NIR Lens. Images were acquired at 5 frames per second. For each larvae,
620 average crawling speed was calculated from long, uninterrupted forward crawls identified
621 manually using FIMTrack. The 15 minute recording period was partitioned into 5 minute
622 sections with each larvae being assayed once within each section, allowing each specimen to
623 be sampled a maximum of 3 times. We observed no change in average crawling speed within
624 the duration of the 15-minute recording.
625

626 **Data Analysis.** All data handling was performed using Prism software (GraphPad). NMJ
627 bouton number and ratiometric ROS reporter data were tested for normal / Gaussian
628 distribution using the D'Agostino-Pearson omnibus normality test. Due to a lower replicate
629 number, dendritic arbor reconstruction data were tested for normality using the

630 Kolmogorov-Smirnov with Dallal-Wilkinson-Lilliefor P value test. Normal distribution was
631 thus confirmed for all data presented, which were compared using one-way analysis of
632 variance (ANOVA), with Tukey's multiple comparisons test where *P<0.05, **P<0.01,
633 ***P<0.001, ****P<0.0001.
634
635

636 ## Figure Supplement Figures

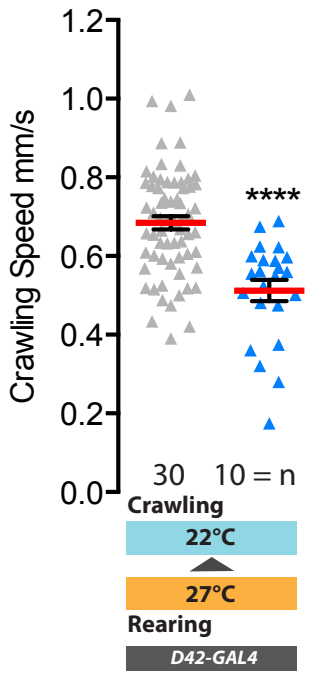

637
638

Figure 1-Figure Supplement 1: Prolonged over-activation targeted to motoneurons (*D42-GAL4*; *UAS-dTrpA1*) also leads to adaptation with reduced crawling speed (dTRPA1 channels open at 27°C, closed at 22°C). Control is *D42-GAL4 / +*. Each data point represents the crawling speed from an individual uninterrupted continuous forward crawl, n = specimen replicate number, up to 3 crawls measured for each larva. ****P<0.0001 students t test.

639

640

641

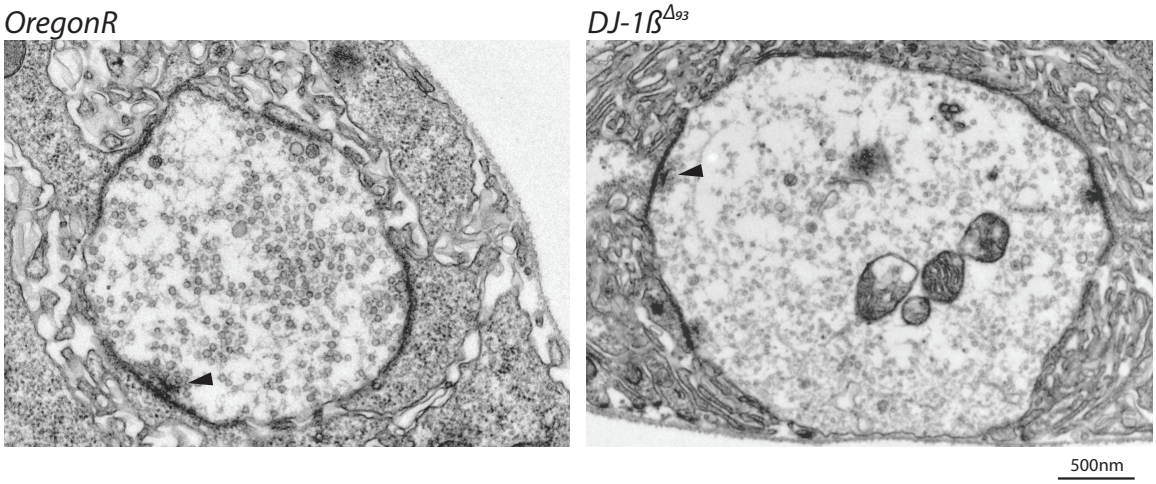

642

Figure 4-Figure Supplement 1: *DJ-1β$^{\Delta 93}$* mutant 3rd instar larval NMJs are phenotypically normal. Representative TEM bouton cross-sectional images showing that pre-synaptic architecture is intact including active-zones with associated clustered synaptic vesicles (arrowed).

643

644

645

646

647

648

649

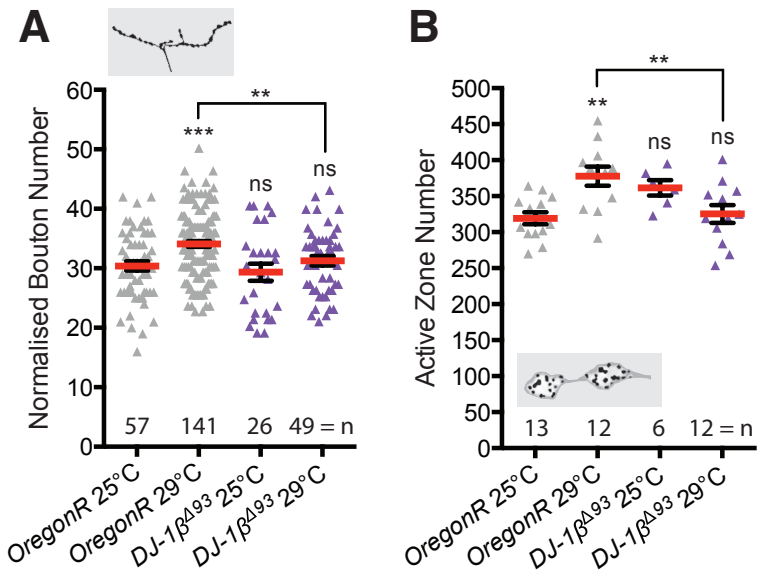

Figure 4-Figure Supplement 2: A. *DJ-1β* null mutant (*DJ-1β*$^{\Delta 93}$) larvae do not show systemic activity-dependent NMJ elaboration. Normalised bouton number dot plot showing significantly increased NMJ elaboration in *OregonR*, but not *DJ-1β*$^{\Delta 93}$, larvae reared at 29°C vs 25°C. **B.** *DJ-1β*$^{\Delta 93}$ larvae also do not show systemic activity-dependent increase in active zone number. *OregonR*, but not *DJ-1β*$^{\Delta 93}$, show significantly increased NMJ active zone number when reared at 29°C vs 25°C. Mean +/- SEM, ANOVA **p<0.01, ***p<0.001, n=replicate number.

References

Albrecht, S.C., Barata, A.G., Grosshans, J., Teleman, A.A., Dick, T.P., 2011. In vivo mapping of hydrogen peroxide and oxidized glutathione reveals chemical and regional specificity of redox homeostasis. Cell Metab 14, 819–829. doi:10.1016/j.cmet.2011.10.010

Ariga, H., Takahashi-Niki, K., Kato, I., Maita, H., Niki, T., Iguchi-Ariga, S.M.M., 2013. Neuroprotective function of DJ-1 in Parkinson's disease. Oxid Med Cell Longev 2013, 683920. doi:10.1155/2013/683920

Ataman, B., Ashley, J., Gorczyca, M., Ramachandran, P., Fouquet, W., Sigrist, S.J., Budnik, V., 2008. Rapid activity-dependent modifications in synaptic structure and function require bidirectional Wnt signaling. Neuron 57, 705–718. doi:10.1016/j.neuron.2008.01.026

Attwell, D., Laughlin, S.B., 2001. An energy budget for signaling in the grey matter of the brain. J. Cereb. Blood Flow Metab. 21, 1133–1145. doi:10.1097/00004647-200110000-00001

Baines, R.A., Robinson, S.G., Fujioka, M., Jaynes, J.B., Bate, M., 1999. Postsynaptic expression of tetanus toxin light chain blocks synaptogenesis in Drosophila. Curr Biol 9, 1267–1270.

Baines, R.A., Uhler, J.P., Thompson, A., Sweeney, S.T., Bate, M., 2001. Altered electrical properties in Drosophila neurons developing without synaptic transmission. J Neurosci 21, 1523–1531.
Bayat, V., Jaiswal, M., Bellen, H.J., 2011. The BMP signaling pathway at the Drosophila neuromuscular junction and its links to neurodegenerative diseases. Curr Opin Neurobiol 21, 182–188. doi:10.1016/j.conb.2010.08.014
Berke, B., Wittnam, J., McNeill, E., Van Vactor, D.L., Keshishian, H., 2013. Retrograde BMP signaling at the synapse: a permissive signal for synapse maturation and activity-dependent plasticity. J Neurosci 33, 17937–17950. doi:10.1523/JNEUROSCI.6075-11.2013
Bindokas, V.P., Jordán, J., Lee, C.C., Miller, R.J., 1996. Superoxide production in rat hippocampal neurons: selective imaging with hydroethidine. J. Neurosci. 16, 1324–1336.
Blackinton, J., Lakshminarasimhan, M., Thomas, K.J., Ahmad, R., Greggio, E., Raza, A.S., Cookson, M.R., Wilson, M.A., 2009. Formation of a stabilized cysteine sulfinic acid is critical for the mitochondrial function of the parkinsonism protein DJ-1. J Biol Chem 284, 6476–6485. doi:10.1074/jbc.M806599200
Bonifati, V., Rizzu, P., van Baren, M.J., Schaap, O., Breedveld, G.J., Krieger, E., Dekker, M.C.J., Squitieri, F., Ibanez, P., Joosse, M., van Dongen, J.W., Vanacore, N., van Swieten, J.C., Brice, A., Meco, G., van Duijn, C.M., Oostra, B.A., Heutink, P., 2003. Mutations in the DJ-1 gene associated with autosomal recessive early-onset parkinsonism. Science 299, 256–259. doi:10.1126/science.1077209
Brennan, A.M., Won Suh, S., Joon Won, S., Narasimhan, P., Kauppinen, T.M., Lee, H., Edling, Y., Chan, P.H., Swanson, R.A., 2009. NADPH oxidase is the primary source of superoxide induced by NMDA receptor activation. Nat Neurosci 12, 857–863. doi:10.1038/nn.2334
Brierley, D.J., Blanc, E., Reddy, O.V., VijayRaghavan, K., Williams, D.W., 2009. Dendritic targeting in the leg neuropil of Drosophila: the role of midline signalling molecules in generating a myotopic map. PLoS Biol 7, e1000199. doi:10.1371/journal.pbio.1000199
Budnik, V., Salinas, P.C., 2011. Wnt signaling during synaptic development and plasticity. Curr Opin Neurobiol 21, 151–159. doi:10.1016/j.conb.2010.12.002
Budnik, V., Zhong, Y., Wu, C.F., 1990. Morphological plasticity of motor axons in Drosophila mutants with altered excitability. J. Neurosci. 10, 3754–3768.
Burrone, J., O'Byrne, M., Murthy, V.N., 2002. Multiple forms of synaptic plasticity triggered by selective suppression of activity in individual neurons. Nature 420, 414–418. doi:10.1038/nature01242
Calì, T., Ottolini, D., Soriano, M.E., Brini, M., 2015. A new split-GFP-based probe reveals DJ-1 translocation into the mitochondrial matrix to sustain ATP synthesis upon nutrient deprivation. Hum Mol Genet 24, 1045–1060. doi:10.1093/hmg/ddu519
Canet-Avilés, R.M., Wilson, M.A., 2004. The Parkinson's disease protein DJ-1 is neuroprotective due to cysteine-sulfinic acid-driven mitochondrial localization, in:. Presented at the Proceedings of the ....
Chandrasekaran, V., Lea, C., Sosa, J.C., Higgins, D., Lein, P.J., 2015. Reactive oxygen species are involved in BMP-induced dendritic growth in cultured rat sympathetic neurons. Mol Cell Neurosci 67, 116–125. doi:10.1016/j.mcn.2015.06.007
Cho, R.W., Buhl, L.K., Volfson, D., Tran, A., Li, F., Akbergenova, Y., Littleton, J.T., 2015. Phosphorylation of Complexin by PKA Regulates Activity-Dependent Spontaneous Neurotransmitter Release and Structural Synaptic Plasticity. Neuron 88, 749–761. doi:10.1016/j.neuron.2015.10.011
Choi, J.C., Park, D., Griffith, L.C., 2004. Electrophysiological and morphological characterization of identified motor neurons in the Drosophila third instar larva central nervous system. J Neurophysiol 91, 2353–2365. doi:10.1152/jn.01115.2003
Crossley, A.C., 1978. Morphology and development of the Drosophila muscular system, in: Ashburner, M., Wright, T. (Eds.), Genetics and Biology of Drosophila. Genetics and biology of Drosophila, New York, pp. 499–560.
Davis, G.W., 2006. Homeostatic control of neural activity: from phenomenology to

molecular design. Annu Rev Neurosci 29, 307–323. doi:10.1146/annurev.neuro.28.061604.135751

Davis, G.W., Davis, G.W., Schuster, C.M., Schuster, C.M., Goodman, C.S., Goodman, C.S., 1996. Genetic dissection of structural and functional components of synaptic plasticity. III. CREB is necessary for presynaptic functional plasticity. Neuron 17, 669–679.

Davis, G.W., DiAntonio, A., Petersen, S.A., Goodman, C.S., 1998. Postsynaptic PKA controls quantal size and reveals a retrograde signal that regulates presynaptic transmitter release in Drosophila. Neuron 20, 305–315.

Davis, G.W., Müller, M., 2015. Homeostatic control of presynaptic neurotransmitter release. Annu Rev Physiol 77, 251–270. doi:10.1146/annurev-physiol-021014-071740

Davydova, D., Marini, C., King, C., Klueva, J., Bischof, F., Romorini, S., Montenegro-Venegas, C., Heine, M., Schneider, R., Schröder, M.S., Altrock, W.D., Henneberger, C., Rusakov, D.A., Gundelfinger, E.D., Fejtova, A., 2014. Bassoon specifically controls presynaptic P/Q-type Ca(2+) channels via RIM-binding protein. Neuron 82, 181–194. doi:10.1016/j.neuron.2014.02.012

Dietzl, G., Chen, D., Schnorrer, F., Su, K.-C., Barinova, Y., Fellner, M., Gasser, B., Kinsey, K., Oppel, S., Scheiblauer, S., Couto, A., Marra, V., Keleman, K., Dickson, B.J., 2007. A genome-wide transgenic RNAi library for conditional gene inactivation in Drosophila. Nature 448, 151–156. doi:10.1038/nature05954

Dillon, M.E., Wang, G., Garrity, P.A., Huey, R.B., 2009. Review: Thermal preference in Drosophila. J. Therm. Biol. 34, 109–119. doi:10.1016/j.jtherbio.2008.11.007

Driscoll, H.E., Muraro, N.I., He, M., Baines, R.A., 2013. Pumilio-2 regulates translation of nav1.6 to mediate homeostasis of membrane excitability. J Neurosci 33, 9644–9654. doi:10.1523/JNEUROSCI.0921-13.2013

Dugan, L.L., Sensi, S.L., Canzoniero, L.M., Handran, S.D., Rothman, S.M., Lin, T.S., Goldberg, M.P., Choi, D.W., 1995. Mitochondrial production of reactive oxygen species in cortical neurons following exposure to N-methyl-D-aspartate. J. Neurosci. 15, 6377–6388.

Evers, J.F., Schmitt, S., Sibila, M., Duch, C., 2005. Progress in functional neuroanatomy: precise automatic geometric reconstruction of neuronal morphology from confocal image stacks. J Neurophysiol 93, 2331–2342. doi:10.1152/jn.00761.2004

Finkel, T., 2011. Signal transduction by reactive oxygen species. J Cell Biol 194, 7–15. doi:10.1083/jcb.201102095

Frank, C.A., Kennedy, M.J., Goold, C.P., Marek, K.W., Davis, G.W., 2006. Mechanisms underlying the rapid induction and sustained expression of synaptic homeostasis. Neuron 52, 663–677. doi:10.1016/j.neuron.2006.09.029

Frank, C.A., Pielage, J., Davis, G.W., 2009. A presynaptic homeostatic signaling system composed of the Eph receptor, ephexin, Cdc42, and CaV2.1 calcium channels. Neuron 61, 556–569. doi:10.1016/j.neuron.2008.12.028

Fujioka, M., Lear, B.C., Landgraf, M., Yusibova, G.L., Zhou, J., Riley, K.M., Patel, N.H., Jaynes, J.B., 2003. Even-skipped, acting as a repressor, regulates axonal projections in Drosophila. Development 130, 5385–5400. doi:10.1242/dev.00770

Funato, Y., Michiue, T., Asashima, M., Miki, H., 2006. The thioredoxin-related redox-regulating protein nucleoredoxin inhibits Wnt-beta-catenin signalling through dishevelled. Nat Cell Biol 8, 501–508. doi:10.1038/ncb1405

Fushiki, A., Zwart, M.F., Kohsaka, H., Fetter, R.D., Cardona, A., Nose, A., 2016. A circuit mechanism for the propagation of waves of muscle contraction in Drosophila. Elife 5. doi:10.7554/eLife.13253

Gahtan, E., Auerbach, J.M., Groner, Y., Segal, M., 1998. Reversible impairment of long-term potentiation in transgenic Cu/Zn-SOD mice. Eur J Neurosci 10, 538–544.

Gao, X., Neufeld, T.P., Pan, D., 2000. Drosophila PTEN regulates cell growth and proliferation through PI3K-dependent and -independent pathways. Dev Biol 221, 404–418. doi:10.1006/dbio.2000.9680

Gaviño, M.A., Ford, K.J., Archila, S., Davis, G.W., 2015. Homeostatic synaptic depression is achieved through a regulated decrease in presynaptic calcium channel abundance. Elife

4. doi:10.7554/eLife.05473
Giachello, C.N., Baines, R.A., 2016. Regulation of motoneuron excitability and the setting of homeostatic limits. Curr Opin Neurobiol 43, 1–6. doi:10.1016/j.conb.2016.09.014
Giniatullin, A.R., Darios, F., Shakirzyanova, A., Davletov, B., Giniatullin, R., 2006. SNAP25 is a pre-synaptic target for the depressant action of reactive oxygen species on transmitter release. J Neurochem 98, 1789–1797. doi:10.1111/j.1471-4159.2006.03997.x
Gjorgjieva, J., Evers, J.F., Eglen, S.J., 2016. Homeostatic Activity-Dependent Tuning of Recurrent Networks for Robust Propagation of Activity. J Neurosci 36, 3722–3734. doi:10.1523/JNEUROSCI.2511-15.2016
Gutscher, M., Sobotta, M.C., Wabnitz, G.H., Ballikaya, S., Meyer, A.J., Samstag, Y., Dick, T.P., 2009. Proximity-based protein thiol oxidation by H2O2-scavenging peroxidases. J Biol Chem 284, 31532–31540. doi:10.1074/jbc.M109.059246
Ha, E.M., 2005. A Direct Role for Dual Oxidase in Drosophila Gut Immunity. Science 310, 847–850. doi:10.1126/science.1117311
Hallermann, S., de Kock, C.P.J., Stuart, G.J., Kole, M.H.P., 2012. State and location dependence of action potential metabolic cost in cortical pyramidal neurons. Nat Neurosci 15, 1007–1014. doi:10.1038/nn.3132
Halliwell, B., 1992. Reactive oxygen species and the central nervous system. J Neurochem 59, 1609–1623.
Hamada, F.N., Hamada, F.N., Rosenzweig, M., Rosenzweig, M., Kang, K., Kang, K., Pulver, S.R., Pulver, S.R., Ghezzi, A., Ghezzi, A., Jegla, T.J., Jegla, T.J., Garrity, P.A., Garrity, P.A., 2008. An internal thermal sensor controlling temperature preference in Drosophila. Nature 454, 217–220. doi:10.1038/nature07001
Hardingham, G.E., Arnold, F.J., Bading, H., 2001. A calcium microdomain near NMDA receptors: on switch for ERK-dependent synapse-to-nucleus communication. Nat Neurosci 4, 565–566. doi:10.1038/88380
Hartwig, C.L., Worrell, J., Levine, R.B., Ramaswami, M., Sanyal, S., 2008. Normal dendrite growth in Drosophila motor neurons requires the AP-1 transcription factor. Dev Neurobiol 68, 1225–1242. doi:10.1002/dneu.20655
Hengen, K.B., Lambo, M.E., Van Hooser, S.D., Katz, D.B., Turrigiano, G.G., 2013. Firing rate homeostasis in visual cortex of freely behaving rodents. Neuron 80, 335–342. doi:10.1016/j.neuron.2013.08.038
Hengen, K.B., Torrado Pacheco, A., McGregor, J.N., Van Hooser, S.D., Turrigiano, G.G., 2016. Neuronal Firing Rate Homeostasis Is Inhibited by Sleep and Promoted by Wake. Cell 165, 180–191. doi:10.1016/j.cell.2016.01.046
Hidalgo, C., Arias-Cavieres, A., 2016. Calcium, Reactive Oxygen Species, and Synaptic Plasticity. Physiology (Bethesda) 31, 201–215. doi:10.1152/physiol.00038.2015
Hongpaisan, J., Winters, C.A., Andrews, S.B., 2004. Strong calcium entry activates mitochondrial superoxide generation, upregulating kinase signaling in hippocampal neurons. J Neurosci 24, 10878–10887. doi:10.1523/JNEUROSCI.3278-04.2004
Hongpaisan, J., Winters, C.A., Andrews, S.B., 2003. Calcium-dependent mitochondrial superoxide modulates nuclear CREB phosphorylation in hippocampal neurons. Molecular and Cellular Neuroscience 24, 1103–1115.
Huddleston, A.T., Tang, W., Takeshima, H., Hamilton, S.L., Klann, E., 2008. Superoxide-induced potentiation in the hippocampus requires activation of ryanodine receptor type 3 and ERK. J Neurophysiol 99, 1565–1571. doi:10.1152/jn.00659.2007
Itakura, Y., Kohsaka, H., Ohyama, T., Zlatic, M., Pulver, S.R., Nose, A., 2015. Identification of Inhibitory Premotor Interneurons Activated at a Late Phase in a Motor Cycle during Drosophila Larval Locomotion. PLoS ONE 10, e0136660. doi:10.1371/journal.pone.0136660
Jindra, M., Gaziova, I., Uhlirova, M., Okabe, M., Hiromi, Y., Hirose, S., 2004. Coactivator MBF1 preserves the redox-dependent AP-1 activity during oxidative stress in Drosophila. EMBO J 23, 3538–3547. doi:10.1038/sj.emboj.7600356
Jordán-Álvarez, S., Fouquet, W., Sigrist, S.J., Acebes, A., 2012. Presynaptic PI3K activity triggers the formation of glutamate receptors at neuromuscular terminals of Drosophila.

835 J Cell Sci 125, 3621–3629. doi:10.1242/jcs.102806
836 Kamsler, A., Segal, M., 2003a. Hydrogen peroxide modulation of synaptic plasticity. J
837 Neurosci 23, 269–276.
838 Kamsler, A., Segal, M., 2003b. Paradoxical actions of hydrogen peroxide on long-term
839 potentiation in transgenic superoxide dismutase-1 mice. J Neurosci 23, 10359–10367.
840 Keck, T., Hübener, M., Bonhoeffer, T., 2017. Interactions between synaptic homeostatic
841 mechanisms: an attempt to reconcile BCM theory, synaptic scaling, and changing
842 excitation/inhibition balance. Curr Opin Neurobiol 43, 87–93.
843 doi:10.1016/j.conb.2017.02.003
844 Keck, T., Keller, G.B., Jacobsen, R.I., Eysel, U.T., Bonhoeffer, T., Hübener, M., 2013.
845 Synaptic scaling and homeostatic plasticity in the mouse visual cortex in vivo. Neuron
846 80, 327–334. doi:10.1016/j.neuron.2013.08.018
847 Kim, R.H., Peters, M., Jang, Y., Shi, W., Pintilie, M., Fletcher, G.C., DeLuca, C., Liepa, J.,
848 Zhou, L., Snow, B., Binari, R.C., Manoukian, A.S., Bray, M.R., Liu, F.-F., Tsao, M.-S.,
849 Mak, T.W., 2005. DJ-1, a novel regulator of the tumor suppressor PTEN. Cancer Cell 7,
850 263–273. doi:10.1016/j.ccr.2005.02.010
851 Kim, S.M., Kumar, V., Lin, Y.-Q., Karunanithi, S., Ramaswami, M., 2009. Fos and Jun
852 potentiate individual release sites and mobilize the reserve synaptic vesicle pool at the
853 Drosophila larval motor synapse. Proc Natl Acad Sci USA 106, 4000–4005.
854 doi:10.1073/pnas.0806064106
855 Kim, Y.-C., Kitaura, H., Taira, T., Iguchi-Ariga, S.M.M., Ariga, H., 2009. Oxidation of DJ-1-
856 dependent cell transformation through direct binding of DJ-1 to PTEN. Int J Oncol 35,
857 1331–1341.
858 Kirov, S.A., Harris, K.M., 1999. Dendrites are more spiny on mature hippocampal neurons
859 when synapses are inactivated. Nat Neurosci 2, 878–883. doi:10.1038/13178
860 Kishida, K.T., Hoeffer, C.A., Hu, D., Pao, M., Holland, S.M., Klann, E., 2006. Synaptic
861 plasticity deficits and mild memory impairments in mouse models of chronic
862 granulomatous disease. Mol Cell Biol 26, 5908–5920. doi:10.1128/MCB.00269-06
863 Kishida, K.T., Pao, M., Holland, S.M., Klann, E., 2005. NADPH oxidase is required for
864 NMDA receptor-dependent activation of ERK in hippocampal area CA1. J Neurochem
865 94, 299–306. doi:10.1111/j.1471-4159.2005.03189.x
866 Klann, E., 1998. Cell-permeable scavengers of superoxide prevent long-term potentiation in
867 hippocampal area CA1. J Neurophysiol 80, 452–457.
868 Knapp, L.T., Klann, E., 2002. Potentiation of hippocampal synaptic transmission by
869 superoxide requires the oxidative activation of protein kinase C. J Neurosci 22, 674–683.
870 Kohsaka, H., Okusawa, S., Itakura, Y., Fushiki, A., Nose, A., 2012. Development of larval
871 motor circuits in Drosophila. Dev Growth Differ 54, 408–419. doi:10.1111/j.1440-
872 169X.2012.01347.x
873 Kohsaka, H., Takasu, E., Morimoto, T., Nose, A., 2014. A group of segmental premotor
874 interneurons regulates the speed of axial locomotion in Drosophila larvae. Curr Biol 24,
875 2632–2642. doi:10.1016/j.cub.2014.09.026
876 Koles, K., Budnik, V., 2012. Wnt signaling in neuromuscular junction development. Cold
877 Spring Harb Perspect Biol 4. doi:10.1101/cshperspect.a008045
878 Landgraf, M., Jeffrey, V., Fujioka, M., Jaynes, J.B., Bate, M., 2003. Embryonic origins of a
879 motor system: motor dendrites form a myotopic map in Drosophila. PLoS Biol 1, E41.
880 doi:10.1371/journal.pbio.0000041
881 Lazarevic, V., Schöne, C., Heine, M., Gundelfinger, E.D., Fejtova, A., 2011. Extensive
882 remodeling of the presynaptic cytomatrix upon homeostatic adaptation to network
883 activity silencing. J Neurosci 31, 10189–10200. doi:10.1523/JNEUROSCI.2088-11.2011
884 Lee, K.Y., Chung, K., Chung, J.M., 2010. Involvement of reactive oxygen species in long-term
885 potentiation in the spinal cord dorsal horn. J Neurophysiol 103, 382–391.
886 doi:10.1152/jn.90906.2008
887 Leevers, S.J., Weinkove, D., MacDougall, L.K., Hafen, E., Waterfield, M.D., 1996. The
888 Drosophila phosphoinositide 3-kinase Dp110 promotes cell growth. EMBO J 15, 6584–
889 6594.

890 Levin, E.D., Brady, T.C., Hochrein, E.C., Oury, T.D., Jonsson, L.M., Marklund, S.L., Crapo,
891 J.D., 1998. Molecular manipulations of extracellular superoxide dismutase: functional
892 importance for learning. Behav. Genet. 28, 381–390.
893 Lin, W.-H., Günay, C., Marley, R., Prinz, A.A., Baines, R.A., 2012. Activity-dependent
894 alternative splicing increases persistent sodium current and promotes seizure. J
895 Neurosci 32, 7267–7277. doi:10.1523/JNEUROSCI.6042-11.2012
896 Loebrich, S., Nedivi, E., 2009. The function of activity-regulated genes in the nervous
897 system. Physiol Rev 89, 1079–1103. doi:10.1152/physrev.00013.2009
898 Love, N.R., Chen, Y., Ishibashi, S., Kritsiligkou, P., Lea, R., Koh, Y., Gallop, J.L., Dorey, K.,
899 Amaya, E., 2013. Amputation-induced reactive oxygen species are required for
900 successful Xenopus tadpole tail regeneration. Nat Cell Biol. doi:10.1038/ncb2659
901 Martín-Peña, A., Acebes, A., Rodríguez, J.-R., Sorribes, A., de Polavieja, G.G., Fernández-
902 Fúnez, P., Ferrús, A., 2006. Age-independent synaptogenesis by phosphoinositide 3
903 kinase. J Neurosci 26, 10199–10208. doi:10.1523/JNEUROSCI.1223-06.2006
904 Matz, J., Gilyan, A., Kolar, A., McCarvill, T., Krueger, S.R., 2010. Rapid structural alterations
905 of the active zone lead to sustained changes in neurotransmitter release. Proc Natl Acad
906 Sci U S A 107, 8836–8841. doi:10.1073/pnas.0906087107
907 Mee, C.J., Pym, E.C.G., Moffat, K.G., Baines, R.A., 2004. Regulation of neuronal excitability
908 through pumilio-dependent control of a sodium channel gene. J Neurosci 24, 8695–
909 8703. doi:10.1523/JNEUROSCI.2282-04.2004
910 Meulener, M., Whitworth, A.J., Armstrong-Gold, C.E., Rizzu, P., Heutink, P., Wes, P.D.,
911 Pallanck, L.J., Bonini, N.M., 2005. Drosophila DJ-1 mutants are selectively sensitive to
912 environmental toxins associated with Parkinson's disease. Curr Biol 15, 1572–1577.
913 doi:10.1016/j.cub.2005.07.064
914 Meulener, M.C., Xu, K., Thomson, L., Thompson, L., Ischiropoulos, H., Bonini, N.M., 2006.
915 Mutational analysis of DJ-1 in Drosophila implicates functional inactivation by oxidative
916 damage and aging. Proc Natl Acad Sci USA 103, 12517–12522.
917 doi:10.1073/pnas.0601891103
918 Milton, V.J., Jarrett, H.E., Gowers, K., Chalak, S., Briggs, L., Robinson, I.M., Sweeney, S.T.,
919 2011. Oxidative stress induces overgrowth of the Drosophila neuromuscular junction.
920 Proc Natl Acad Sci U S A 108, 17521–17526. doi:10.1073/pnas.1014511108
921 Milton, V.J., Sweeney, S.T., 2012. Oxidative stress in synapse development and function. Dev
922 Neurobiol 72, 100–110. doi:10.1002/dneu.20957
923 Missirlis, F., Phillips, J.P., Jäckle, H., 2001. Cooperative action of antioxidant defense
924 systems in Drosophila. Current Biology 11, 1272–1277.
925 Missirlis, F., Rahlfs, S., Dimopoulos, N., Bauer, H., Becker, K., Hilliker, A., Phillips, J.P.,
926 Jäckle, H., 2003. A putative glutathione peroxidase of Drosophila encodes a thioredoxin
927 peroxidase that provides resistance against oxidative stress but fails to complement a
928 lack of catalase activity. Biol Chem 384, 463–472. doi:10.1515/BC.2003.052
929 Murthy, V.N., Schikorski, T., Stevens, C.F., Zhu, Y., 2001. Inactivity produces increases in
930 neurotransmitter release and synapse size. Neuron 32, 673–682.
931 Müller, M., Davis, G.W., 2012. Transsynaptic control of presynaptic Ca^{2+} influx achieves
932 homeostatic potentiation of neurotransmitter release. Curr Biol 22, 1102–1108.
933 doi:10.1016/j.cub.2012.04.018
934 Nagakubo, D., Taira, T., Kitaura, H., Ikeda, M., Tamai, K., Iguchi-Ariga, S.M., Ariga, H.,
935 1997. DJ-1, a novel oncogene which transforms mouse NIH3T3 cells in cooperation with
936 ras. Biochem Biophys Res Commun 231, 509–513. doi:10.1006/bbrc.1997.6132
937 O'Leary, T., Williams, A.H., Caplan, J.S., Marder, E., 2013. Correlations in ion channel
938 expression emerge from homeostatic tuning rules. Proc Natl Acad Sci U S A 110, E2645–
939 54. doi:10.1073/pnas.1309966110
940 O'Leary, T., Williams, A.H., Franci, A., Marder, E., 2014. Cell types, network homeostasis,
941 and pathological compensation from a biologically plausible ion channel expression
942 model. Neuron 82, 809–821. doi:10.1016/j.neuron.2014.04.002
943 Osses, N., Henriquez, J.P., 2014. Bone morphogenetic protein signaling in vertebrate motor
944 neurons and neuromuscular communication. Front Cell Neurosci 8, 453.

doi:10.3389/fncel.2014.00453
Ou, Y., Chwalla, B., Landgraf, M., van Meyel, D.J., 2008. Identification of genes influencing dendrite morphogenesis in developing peripheral sensory and central motor neurons. Neural development 3, 16. doi:10.1186/1749-8104-3-16
Peled, E.S., Newman, Z.L., Isacoff, E.Y., 2014. Evoked and spontaneous transmission favored by distinct sets of synapses. Curr Biol 24, 484–493. doi:10.1016/j.cub.2014.01.022
Peng, T.-I., Jou, M.-J., 2010. Oxidative stress caused by mitochondrial calcium overload. Ann N Y Acad Sci 1201, 183–188. doi:10.1111/j.1749-6632.2010.05634.x
Piccioli, Z.D., Littleton, J.T., 2014. Retrograde BMP Signaling Modulates Rapid Activity-Dependent Synaptic Growth via Presynaptic LIM Kinase Regulation of Cofilin. J Neurosci 34, 4371–4381. doi:10.1523/JNEUROSCI.4943-13.2014
Prinz, A.A., 2006. Insights from models of rhythmic motor systems. Curr Opin Neurobiol 16, 615–620. doi:10.1016/j.conb.2006.10.001
Prinz, A.A., Bucher, D., Marder, E., 2004. Similar network activity from disparate circuit parameters. Nat Neurosci 7, 1345–1352. doi:10.1038/nn1352
Pulver, S.R., Pulver, S.R., Pashkovski, S.L., Pashkovski, S.L., Hornstein, N.J., Hornstein, N.J., Garrity, P.A., Garrity, P.A., Griffith, L.C., Griffith, L.C., 2009. Temporal dynamics of neuronal activation by Channelrhodopsin-2 and TRPA1 determine behavioral output in Drosophila larvae. J Neurophysiol 101, 3075–3088. doi:10.1152/jn.00071.2009
Rharass, T., Lemcke, H., Lantow, M., Kuznetsov, S.A., Weiss, D.G., Panáková, D., 2014. Ca2+-mediated mitochondrial reactive oxygen species metabolism augments Wnt/β-catenin pathway activation to facilitate cell differentiation. J Biol Chem 289, 27937–27951. doi:10.1074/jbc.M114.573519
Risse, B., Thomas, S., Otto, N., Löpmeier, T., Valkov, D., Jiang, X., Klämbt, C., 2013. FIM, a Novel FTIR-Based Imaging Method for High Throughput Locomotion Analysis. PLoS ONE 8, e53963. doi:10.1371/journal.pone.0053963
Roy, B., Singh, A.P., Shetty, C., Chaudhary, V., North, A., Landgraf, M., VijayRaghavan, K., Rodrigues, V., 2007. Metamorphosis of an identified serotonergic neuron in the Drosophila olfactory system. Neural development 2, 20. doi:10.1186/1749-8104-2-20
Sanyal, S., Narayanan, R., Consoulas, C., Ramaswami, M., 2003. Evidence for cell autonomous AP1 function in regulation of Drosophila motor-neuron plasticity. BMC neuroscience 4, 20. doi:10.1186/1471-2202-4-20
Sanyal, S., Sandstrom, D.J., Hoeffer, C.A., Ramaswami, M., 2002. AP-1 functions upstream of CREB to control synaptic plasticity in Drosophila. Nature 416, 870–874. doi:10.1038/416870a
Schmitt, S., Evers, J.F., Duch, C., Scholz, M., Obermayer, K., 2004. New methods for the computer-assisted 3-D reconstruction of neurons from confocal image stacks. Neuroimage 23, 1283–1298. doi:10.1016/j.neuroimage.2004.06.047
Schneider-Mizell, C.M., Gerhard, S., Longair, M., Kazimiers, T., Li, F., Zwart, M.F., Champion, A., Midgley, F.M., Fetter, R.D., Saalfeld, S., Cardona, A., 2016. Quantitative neuroanatomy for connectomics in Drosophila. Elife 5. doi:10.7554/eLife.12059
Schuster, C.M., Schuster, C.M., Davis, G.W., Davis, G.W., Fetter, R.D., Fetter, R.D., Goodman, C.S., Goodman, C.S., 1996. Genetic dissection of structural and functional components of synaptic plasticity. I. Fasciclin II controls synaptic stabilization and growth. Neuron 17, 641–654.
Serrano, F., Kolluri, N.S., Wientjes, F.B., Card, J.P., Klann, E., 2003. NADPH oxidase immunoreactivity in the mouse brain. Brain Res 988, 193–198.
Shearin, H.K., Macdonald, I.S., Spector, L.P., Stowers, R.S., 2014. Hexameric GFP and mCherry Reporters for the Drosophila GAL4, Q, and LexA Transcription Systems. Genetics 196, 951–960. doi:10.1534/genetics.113.161141
Sigrist, S.J., Reiff, D.F., Thiel, P.R., Steinert, J.R., Schuster, C.M., 2003. Experience-dependent strengthening of Drosophila neuromuscular junctions. J Neurosci 23, 6546–6556.
Sugie, A., Hakeda-Suzuki, S., Suzuki, E., Silies, M., Shimozono, M., Möhl, C., Suzuki, T.,

Tavosanis, G., 2015. Molecular Remodeling of the Presynaptic Active Zone of Drosophila Photoreceptors via Activity-Dependent Feedback. Neuron 86, 711–725. doi:10.1016/j.neuron.2015.03.046

Sulkowski, M., Kim, Y.-J., Serpe, M., 2014. Postsynaptic glutamate receptors regulate local BMP signaling at the Drosophila neuromuscular junction. Development 141, 436–447. doi:10.1242/dev.097758

Tantama, M., Martínez-François, J.R., Mongeon, R., Yellen, G., 2013. Imaging energy status in live cells with a fluorescent biosensor of the intracellular ATP-to-ADP ratio. Nat Comms 4, 2550. doi:10.1038/ncomms3550

Tejada-Simon, M.V., Serrano, F., Villasana, L.E., Kanterewicz, B.I., Wu, G.Y., Quinn, M.T., Klann, E., 2005. Synaptic localization of a functional NADPH oxidase in the mouse hippocampus. Molecular and Cellular Neuroscience 29, 97–106. doi:10.1016/j.mcn.2005.01.007

Thiels, E., Urban, N.N., Gonzalez-Burgos, G.R., Kanterewicz, B.I., Barrionuevo, G., Chu, C.T., Oury, T.D., Klann, E., 2000. Impairment of long-term potentiation and associative memory in mice that overexpress extracellular superoxide dismutase. J Neurosci 20, 7631–7639.

Tripodi, M., Evers, J.F., Mauss, A., Bate, M., Landgraf, M., 2008. Structural homeostasis: compensatory adjustments of dendritic arbor geometry in response to variations of synaptic input. PLoS Biol 6, e260. doi:10.1371/journal.pbio.0060260

Turrigiano, G., 2012. Homeostatic synaptic plasticity: local and global mechanisms for stabilizing neuronal function. Cold Spring Harb Perspect Biol 4, a005736. doi:10.1101/cshperspect.a005736

Van Vactor, D., Sigrist, S.J., 2017. Presynaptic morphogenesis, active zone organization and structural plasticity in Drosophila. Curr Opin Neurobiol 43, 119–129. doi:10.1016/j.conb.2017.03.003

Vasin, A., Zueva, L., Torrez, C., Volfson, D., Littleton, J.T., Bykhovskaia, M., 2014. Synapsin regulates activity-dependent outgrowth of synaptic boutons at the Drosophila neuromuscular junction. J Neurosci 34, 10554–10563. doi:10.1523/JNEUROSCI.5074-13.2014

Vonhoff, F., Keshishian, H., 2017. Activity-Dependent Synaptic Refinement: New Insights from Drosophila. Front Syst Neurosci 11, 23. doi:10.3389/fnsys.2017.00023

Waak, J., Weber, S.S., Görner, K., Schall, C., Ichijo, H., Stehle, T., Kahle, P.J., 2009. Oxidizable residues mediating protein stability and cytoprotective interaction of DJ-1 with apoptosis signal-regulating kinase 1. J Biol Chem 284, 14245–14257. doi:10.1074/jbc.M806902200

Walker, J.A., Gouzi, J.Y., Long, J.B., Huang, S., Maher, R.C., Xia, H., Khalil, K., Ray, A., Van Vactor, D., Bernards, R., Bernards, A., 2013. Genetic and Functional Studies Implicate Synaptic Overgrowth and Ring Gland cAMP/PKA Signaling Defects in the Drosophila melanogaster Neurofibromatosis-1 Growth Deficiency. PLoS Genet 9, e1003958. doi:10.1371/journal.pgen.1003958

Wang, T., Hauswirth, A.G., Tong, A., Dickman, D.K., Davis, G.W., 2014. Endostatin Is a Trans-Synaptic Signal for Homeostatic Synaptic Plasticity. Neuron. doi:10.1016/j.neuron.2014.07.003

Wefelmeyer, W., Cattaert, D., Burrone, J., 2015. Activity-dependent mismatch between axo-axonic synapses and the axon initial segment controls neuronal output. Proc Natl Acad Sci U S A 112, 9757–9762. doi:10.1073/pnas.1502902112

Weyhersmüller, A., Hallermann, S., Wagner, N., Eilers, J., 2011. Rapid active zone remodeling during synaptic plasticity. J Neurosci 31, 6041–6052. doi:10.1523/JNEUROSCI.6698-10.2011

Younger, M.A., Müller, M., Tong, A., Pym, E.C., Davis, G.W., 2013. A presynaptic ENaC channel drives homeostatic plasticity. Neuron 79, 1183–1196. doi:10.1016/j.neuron.2013.06.048

Zhong, Y., Wu, C.-F., 2004. Neuronal Activity and Adenylyl Cyclase in Environment-Dependent Plasticity of Axonal Outgrowth in Drosophila. J Neurosci 24, 1439–1445.

1055 doi:10.1523/JNEUROSCI.0740-02.2004
1056 Zhu, X.-H., Qiao, H., Du, F., Xiong, Q., Liu, X., Zhang, X., Ugurbil, K., Chen, W., 2012.
1057 Quantitative imaging of energy expenditure in human brain. Neuroimage 60, 2107–2117.
1058 doi:10.1016/j.neuroimage.2012.02.013
1059 Zito, K., Parnas, D., Fetter, R.D., Isacoff, E.Y., Goodman, C.S., 1999. Watching a synapse
1060 grow: noninvasive confocal imaging of synaptic growth in Drosophila. Neuron 22, 719–
1061 729.
1062 Zuo, Y., Lin, A., Chang, P., Gan, W.-B., 2005. Development of long-term dendritic spine
1063 stability in diverse regions of cerebral cortex. Neuron 46, 181–189.
1064 doi:10.1016/j.neuron.2005.04.001
1065 Zwart, M.F., Pulver, S.R., Truman, J.W., Fushiki, A., Fetter, R.D., Cardona, A., Landgraf, M.,
1066 2016. Selective Inhibition Mediates the Sequential Recruitment of Motor Pools. Neuron
1067 91, 944. doi:10.1016/j.neuron.2016.07.041
1068 Zwart, M.F., Randlett, O., Evers, J.F., Landgraf, M., 2013. Dendritic growth gated by a
1069 steroid hormone receptor underlies increases in activity in the developing Drosophila
1070 locomotor system. Proc Natl Acad Sci U S A. doi:10.1073/pnas.1311711110
1071